

Review

Design, Synthesis, and Biomedical Application of Multifunctional Fluorescent Polymer Nanomaterials

Qingpan Bu ¹, Ping Li ¹, Yunfei Xia ¹, Die Hu ¹, Wenjing Li ², Dongfang Shi ^{3,*} and Kai Song ^{1,3,*} 

¹ School of Life Science, Changchun Normal University, Changchun 130032, China; buqingpan@ccsfu.edu.cn (Q.B.); chunlps@163.com (P.L.); xiayunfei1103@163.com (Y.X.); hudie18784775519@163.com (D.H.)

² School of Education, Changchun Normal University, Changchun 130032, China; liwenj678@163.com

³ Institute of Science, Technology and Innovation, Changchun Normal University, Changchun 130032, China

* Correspondence: shidongfang@ccsfu.edu.cn (D.S.); songkai@ccsfu.edu.cn (K.S.)

Abstract: Luminescent polymer nanomaterials not only have the characteristics of various types of luminescent functional materials and a wide range of applications, but also have the characteristics of good biocompatibility and easy functionalization of polymer nanomaterials. They are widely used in biomedical fields such as bioimaging, biosensing, and drug delivery. Designing and constructing new controllable synthesis methods for multifunctional fluorescent polymer nanomaterials with good water solubility and excellent biocompatibility is of great significance. Exploring efficient functionalization methods for luminescent materials is still one of the core issues in the design and development of new fluorescent materials. With this in mind, this review first introduces the structures, properties, and synthetic methods regarding fluorescent polymeric nanomaterials. Then, the functionalization strategies of fluorescent polymer nanomaterials are summarized. In addition, the research progress of multifunctional fluorescent polymer nanomaterials for bioimaging is also discussed. Finally, the synthesis, development, and application fields of fluorescent polymeric nanomaterials, as well as the challenges and opportunities of structure–property correlations, are comprehensively summarized and the corresponding perspectives are well illustrated.



Citation: Bu, Q.; Li, P.; Xia, Y.; Hu, D.; Li, W.; Shi, D.; Song, K. Design, Synthesis, and Biomedical Application of Multifunctional Fluorescent Polymer Nanomaterials. *Molecules* **2023**, *28*, 3819. <https://doi.org/10.3390/molecules28093819>

Academic Editors: Sudeshna Chandra and Heinrich Lang

Received: 12 April 2023

Revised: 24 April 2023

Accepted: 27 April 2023

Published: 29 April 2023



Copyright: © 2023 by the authors. Licensee MDPI, Basel, Switzerland. This article is an open access article distributed under the terms and conditions of the Creative Commons Attribution (CC BY) license (<https://creativecommons.org/licenses/by/4.0/>).

Keywords: light-emitting polymer nanomaterials; rare earth polymers; semiconducting polymers; organic fluorescent small molecule cell imaging; biomedical imaging

1. Introduction

Bioluminescent imaging is a visual imaging method that detects the intrinsic fluorescence of organisms, or the intensity of fluorescence luminescence after fluorescent materials mark organisms. Compared with traditional medical diagnostic imaging methods, it has the characteristics of fast imaging speed, high resolution, and applying no radiation damage to organisms. Applications can range from micron-sized cells to large-sized living organisms [1–3]. After years of research and development, commercial bioluminescence imaging systems are now widely used in the biomedical field, including laser scanning confocal microscopes, two-photon laser scanning microscopy imaging systems, and in vivo fluorescence imaging techniques. In combination with traditional biological imaging techniques such as magnetic resonance imaging (MRI), ultrasonic imaging (US), and computed tomography (CT), etc., the functions are complementary, and more accurate and effective biological imaging can be achieved, providing a reliable imaging method for the early diagnosis of cancer [4–6].

At present, fluorescent imaging materials mainly include inorganic fluorescent functional materials (quantum dots, rare earth luminescent materials, noble metal nanomaterials, etc.) and organic fluorescent functional materials (organic small molecule fluorescent materials and semiconducting polymers) [7–9]. Among them, quantum dots have good fluorescence quantum efficiency and photostability, but cannot avoid the biological toxicity

of heavy metals [10,11]. Organic small molecule fluorescent dyes are the most widely used class of fluorescent materials. However, due to the disadvantages of poor stability, easy photobleaching, small Stokes shift and short fluorescence lifetime, its application range is greatly limited [12]. Rare earth luminescent materials, compared with other fluorescent polymer materials, have a narrow emission band (10–20 nm) and a large Stokes shift. The emission lifetime from microseconds to milliseconds can be achieved, which greatly reduces the interference of the self-luminous background of biological tissues. However, the material itself has poor biocompatibility, and it is prone to fluorescence aggregation quenching or quenching by water in a physiological environment [13,14]. Semiconducting polymers also have many excellent characteristics, for example, good photostability and photothermal performance, easy functional modification of the surface of the material, and good biocompatibility. However, the molecular weight is not easy to control during the preparation process, and the metabolic mechanism in the human body is still unclear [15,16].

Fluorescent polymer nanomaterials are prepared by physically doping or chemically bonding amphiphilic block polymers and fluorescent functional materials [17,18]. The composite material has the characteristics of good optical stability and wide application range of functional fluorescent materials. Additionally, it is also possible to select polymer monomers with different functions; while retaining the good water solubility and excellent biocompatibility of polymer nanomaterials, the controllable synthesis of properties such as size, morphology, stability, and surface properties can be achieved [19,20]. The complementary advantages of the two provide new ideas for expanding the application range of fluorescent functional materials in the field of biomedicine and have attracted the extensive attention of scientific researchers [21–23].

In summary, this paper discusses the functionalization strategy of fluorescent polymers and the preparation methods for fluorescent polymer nanomaterials. It also systematically introduces the research and development status and application prospects of fluorescent polymer nanomaterials based on rare earth luminescent materials, semiconducting polymers, and small organic molecules from recent years. It is emphasized that the design and application of fluorescent polymer nanomaterials should be functionalized from the perspective of synthesis and optimization according to need. Finally, the development direction and challenges of polymer nanomaterials in the fields of optics and medical tumors are prospected.

2. Fluorescent Polymer Functionalization Strategy

Ideal bioluminescent imaging probes, in addition to high fluorescence efficiency and stable luminescent properties, also need to have good monodispersity in aqueous systems. They have low toxicity to biological organisms and active groups on the surface to facilitate the connection of targeting molecules, achieving the effect of targeted imaging [24–26]. However, quantum dots of inorganic functional fluorescent materials, rare earth luminescent materials and noble metal nanoclusters, and semiconducting polymers of organic fluorescent functional materials and organic small molecule fluorescent materials have poor compatibility, poor degradability and long-term biological toxicity in vivo, and other defects. These problems severely limit their application in the biological field [27,28].

Fluorescent polymer nanomaterials are prepared by combining amphiphilic polymers and fluorescent functional materials using physical doping or covalent linkage. They not only have the characteristics of good optical stability and wide application range of fluorescent functional materials but can also be polymerized by selecting different functional monomers [29,30]. While retaining the good water solubility and excellent biocompatibility of polymer nanomaterials, the controllable synthesis of properties such as size, shape, stability, and surface properties can be achieved. As shown in Figure 1, the currently commonly used strategies for functional modification of fluorescent polymers mainly include physical encapsulation and covalent linkage [31–33].

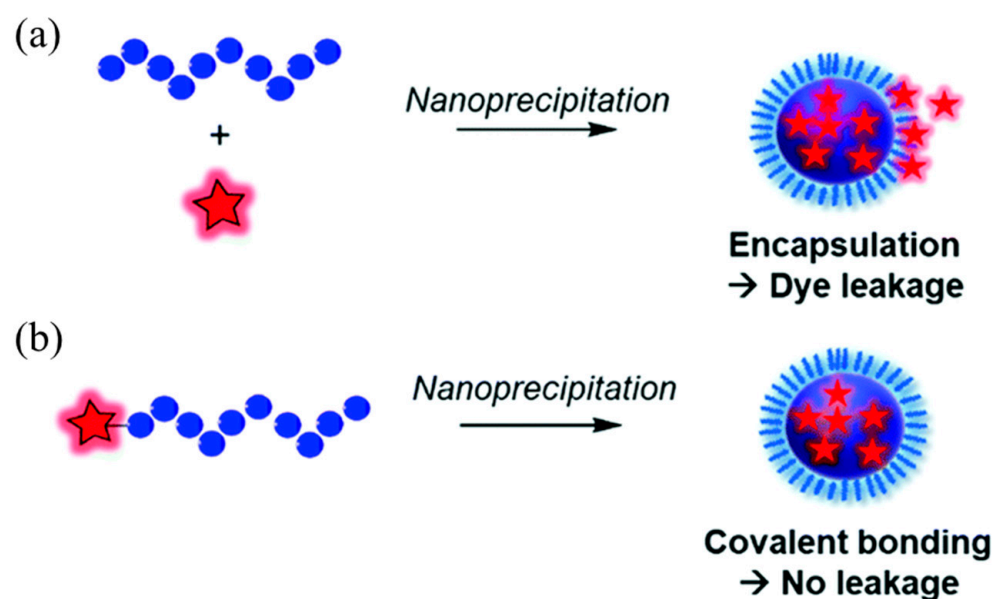


Figure 1. Schematic diagram of the preparation of fluorescent polymer nanoparticles: (a) physical encapsulation; (b) covalent attachment [31]. Copyright (2021), with permission from Royal Society of Chemistry.

2.1. Physical Package

Physical encapsulation is the most commonly used method at present. Fluorescent functional materials are directly embedded in polymer nanoparticles using physical encapsulation to prepare fluorescent polymer nanoparticles. The nanoparticles belong to a typical core-shell structure, in which the hydrophilic polymer acts as a protective layer in the shell, and the hydrophobic fluorescent material acts as a fluorescent chromophore in the core. It not only retains the luminescent properties of fluorescent materials, but also improves the stability and biocompatibility of hydrophobic fluorescent materials in water systems [34–36]. Yu et al. [37] designed and synthesized a semiconducting polymer PDFT based on diketopyrrolopyrrole (DPP). As shown in Figure 2, the amphiphilic distearoylphosphatidylethanolamine-polyethylene glycol (DSPE-mPEG) was used for physical encapsulation. Self-assembled into an NIR-II fluorescent nanoprobe PDFT1032 with a particle size of 68 nm, the maximum emission wavelength is 1032 nm, and it has excellent photostability, excellent biocompatibility, and extremely low in vivo toxicity. It presents high-resolution, real-time imaging in tumor diagnosis and vascular thrombosis treatment and, more importantly, realizes precise fluorescence imaging “navigation” for in situ tumor surgery and sentinel lymph node biopsy.

If the fluorescent material has hydrophobic properties, the preparation method of physical encapsulation can be used, which has good universality. However, due to the absence of chemical bonds between the polymer and the fluorescent-emitting group, there are situations where the fluorescent material leaks from the fluorescent polymer composite system or the aggregation and quenching of the local fluorescent material occurs, resulting in a decrease in luminescent performance [38,39]. Therefore, how to improve the preparation of fluorescent polymer nanoparticles with stable luminescence using physical encapsulation is still a research hotspot.

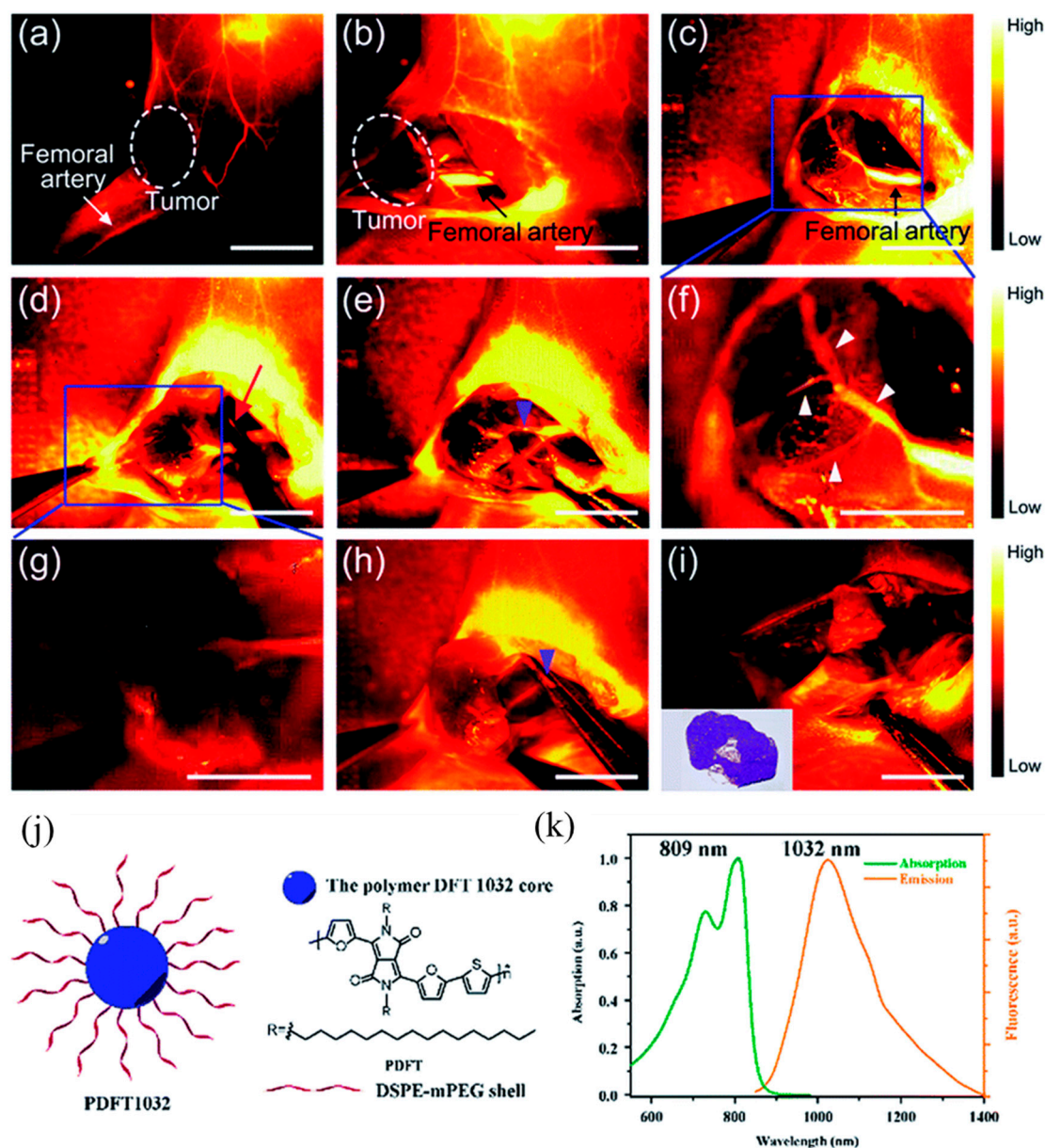


Figure 2. Schematic of DPP-based semiconducting polymer PDFT nanoscale self-assembly and imaging. (a) The vascular mapping and the hemodynamic status of the tumor and the femoral artery were determined. The white dashed circle contours the location of the tumor. (b,c) The branch of the femoral artery that supports the tumor and the vascular network of the tumor (exhibited as a claw shape) were clearly identified. (d) A vessel clamp was used to block the blood flow (red arrow) and the signal of the vascular network vanished. (e) After 5 min, the clamp was removed and the blood flow of the tumor was still devoid because a temporary thrombus was formed (blue arrowhead). (f) Magnification of (c). The vascular network of the tumor was clearly identified (white arrowheads). (g) Magnification of (d). (h) The major artery was surgically incised (blue arrowhead). (i) NIR-II imaging exhibited the absence of the residual tumor fluorescence and normal circulation (femoral artery) was successfully maintained. Inset is the histological analysis of the osteosarcoma. Scale bar: 8 mm. (j) Schematic drawing of a PDFT1032 nanoparticle composed of semiconducting polymer DFT and a hydrophilic DSPE-mPEG shell. (k) Absorbance and fluorescence spectrum of PDFT1032 showing an absorption peak at 809 nm and a fluorescence peak at 1032 nm with an 808 nm excitation laser [37]. Copyright (2018), with permission from Royal Society of Chemistry.

2.2. Covalent Linkage

There are two ways to prepare covalently linked fluorescent polymer nanomaterials [31,40]: one is to first copolymerize polymer monomers into polymer chains, and then use covalently linked methods. The fluorescent-emitting group is attached to the polymer chain, and then prepared into nanoparticles. As shown in Figure 3a, it is referred to as “aggregate first and then join”. The nanoparticles prepared in this way have good stability, and the desired multifunctional nanoparticles can be customized by selecting different polymer nanoparticles. However, this preparation method requires functional group matching between empty polymer nanoparticles and fluorescent groups, and its universality is slightly worse than physical packaging. In addition, fluorescent group materials are also prone to fluorescence quenching on the surface of nanoparticles [41,42]. The second approach is to prepare fluorescent groups and polymer monomers into fluorescent polymer monomers, then copolymerize and self-assemble them into fluorescent polymer nanomaterials, as shown in Figure 3b, referred to as “connection first and then polymerization”. The distribution of light-emitting groups in the fluorescent nanoparticles prepared using this method is relatively more uniform, and the optical stability is good. However, there is also the problem that the size of fluorescent polymer nanoparticles is not easy to control due to the steric hindrance of the luminescent group [43,44].

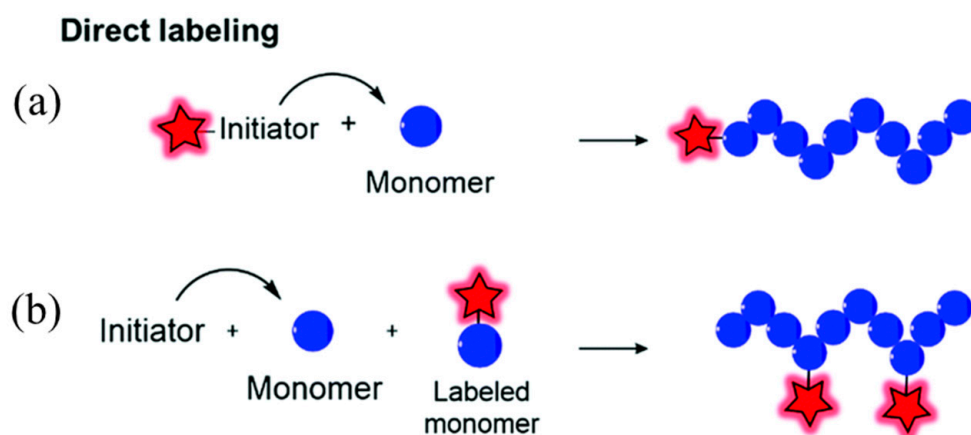


Figure 3. Two forms of covalent linkage: (a) polymerization followed by linkage; (b) linkage followed by aggregation [31]. Copyright (2021), with permission from Royal Society of Chemistry.

In summary, although the method of physical packaging is used to prepare fluorescent polymer nanomaterials, the distribution of fluorescent materials in nanomaterials is uneven and leaks easily. However, it is still the most commonly used method at present. In order to solve the above problems, designing and synthesizing new fluorescent polymer nanomaterials by means of covalent linkage is still one of the hotspots of scientific research.

3. Preparation Method of Fluorescent Polymer Nanomaterials

3.1. Active/Controllable Synthesis of Amphiphilic Block Polymers

From the preparation strategy of fluorescent polymer nanomaterials in the previous section, it can be seen that the controllable synthesis of amphiphilic block polymers directly determines the monodispersity, morphology, and size of bioluminescent probes in aqueous solution. At present, the most commonly used living/controllable polymerization methods mainly include atom transfer radical polymerization (ATRP) [45,46] and reversible addition–fragmentation chain transfer polymerization (RAFT) [47]. Below, we focus on the introduction of these two technologies, as shown in Table 1.

Table 1. Comparison of different preparation strategies for fluorescent polymer materials.

Synthesis Technology		Advantages	Disadvantages
Living/controllable synthesis of amphiphilic block polymers	ATRP	The reaction temperature is mild, the operation is simple, and it is easy to industrialize.	The intermediate process is completely uncontrolled; the amount of transition metal complex is large; the aging of the polymer.
	RAFT	It has a wide range of applications, good polymerization ability, and the molecular weight of the obtained polymer is uniform.	Few applicable monomers, limited scope of molecular design, expensive.
	Nanoprecipitation	Simple operation, fast, high reproducibility, good dispersion of colloidal nanoparticles and easy functionalization.	There are fewer types of polymers, and the process of particle growth is not easy to control.
Physical package	Microemulsion method	Narrow particle size distribution, controllable, good stability.	Surfactants are difficult to remove and have large particle sizes.
	Self-assembly method	It is very convenient to prepare various exotic three-dimensional structures; it is also possible to prepare porous materials that inherit the original morphology and structure	Unstable under physiological conditions.
Covalent linkage	PISA	The process is simple, the price adjustment is gentle, and nano-medicine can be prepared in one step.	The operation is complicated, the reaction takes a long time, and the concentration of the prepared nanoparticles is low (≤ 1 mg/mL), which makes it impossible to achieve large-scale mass production.
	Precipitation polymerization	The particle size of the polymer is uniform and clean, the viscosity of the polymerization system is low, and no surfactant and stabilizer are needed.	Low microspheres yield and high solvent toxicity.

3.1.1. ATRP

Matyjaszewski et al. [48] and Sawamoto et al. [49] successively proposed the method of atom transfer radical polymerization (ATRP). The low-valence metal complex M_t^n takes an electron from the initiator organic halide R-X to form R free radicals to initiate monomer aggregation. The formation of chain free radicals P can also take the halogen atom X from the high-valence metal halide $M_t^{n+1}-X$ passivation to P-X, and reduce the high-valence metal halide to M_t^n . The reversible transfer equilibrium reaction between the free radical active seeds and the halide dormant seeds of the polymer chains enables effective control of the reactions. Compared with the traditional free radical polymerization, the ATRP method has a wide range of adaptability, can control the molecular weight distribution (PDI) of the polymer between 1.05 and 1.5, and has a mild reaction temperature, simple operation, and is easy to industrialize [50–52]. However, when applied to the synthesis of bioluminescent probes, copper-based catalysts have high biotoxicity, and finding other catalysts to replace copper-based catalysts is still a hotspot in ATRP research [53].

3.1.2. RAFT

Compared with the ATRP reaction, the reversible addition–fragmentation chain transfer polymerization (RAFT) reaction system does not involve the participation of copper-based and other biologically toxic transition metals. Additionally, the source of free radicals is basically from the decomposition of organic initiators. For example, azobisisobutyronitrile (AIBN) or dibenzoyl peroxide (BPO) are more suitable for the controlled synthesis of amphiphilic block polymers for biological use [54,55].

The RAFT method was proposed by Rizzardo [56]. The first is initiation (initiation), where the initiator generates free radicals I, then monomers M are initiated to polymerize

with each other to generate extended chain free radicals P_n . The second step is the chain transfer reaction (chain transfer); the extended chain free radical P_n reacts with the dithioester chain transfer agent (1) to form an unstable intermediate (2). The groups on both sides of the intermediate can be broken to form a temporarily inactive thioester dormant (3) and a new free radical $R\cdot$. The third step is to reinitiate the polymerization between the new free radical $R\cdot$ and the monomer to form $P_m\cdot$ (re-initiation). The fourth step is the process of chain equilibrium (chain equilibration), and the macromolecular chain transfer agent (macro-CTA) plays a controlling role. The free radical concentration is low throughout the reaction. Therefore, the molecular weight distribution of the polymer is relatively uniform. The final termination reaction (termination) generally quenches the reaction directly at low temperature, and the product is a mainly macromolecular chain transfer [57,58].

The RAFT mechanism is applicable to a wide range of monomers. The reaction temperature is 60–70 °C, and it has good polymerization ability for monomers such as acrylic acid (AA), methacrylic acid (MAA), and methyl methacrylate (MMA). The resulting polymers are of uniform molecular weight (PDI typically below 1.3). However, this reaction relies heavily on expensive RAFT reagents, and the development of stable, low-cost, and easy-to-synthesize RAFT reagents that meet different systems is still one of the research hotspots [59–61].

3.2. Preparation Method of Physically Encapsulating Fluorescent Polymer Nanoparticles

From the perspective of preparation strategy, fluorescent polymer nanoparticles wrap luminescent materials into amphiphilic block polymers using physical doping. Nanoprecipitation, microemulsion, and self-assembly methods are commonly used, which are similar to the preparation methods of semiconducting polymer nanomaterials, as shown in Figure 4 [62,63].

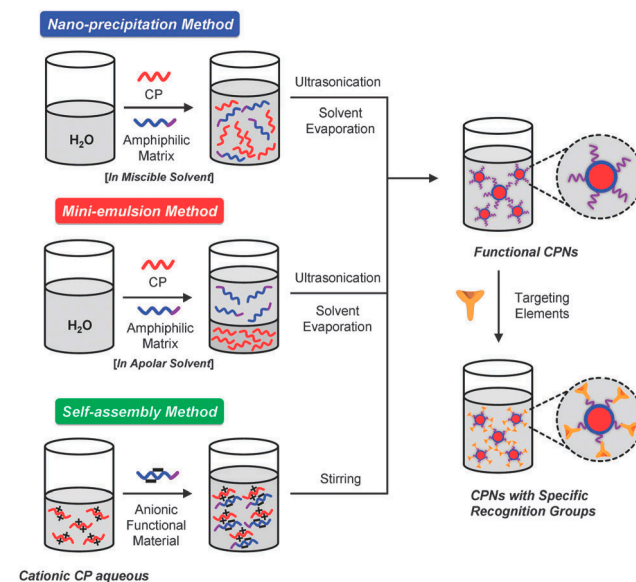


Figure 4. Preparation method for semiconducting polymer nanoparticles [63]. Copyright (2013), with permission from Royal Society of Chemistry.

Nanoprecipitation is a method based on the interfacial deposition of polymers. It was first proposed by Masuhara et al. [64] and then improved by McNeill [65] and Chiu [66]. It is widely used in the preparation of fluorescent nanoparticles in the biological field. Firstly, the fluorescent material and the amphiphilic block polymer material are dissolved in a small amount of good solvent. The material is quickly dropped into a poor solvent (usually deionized water) with vigorous stirring or ultrasound; the huge difference in solubility of the two solvents promotes the aggregation of polymer materials to form nanoparticles, with a particle size of about 15 nm. The process of nanoparticle formation mainly includes

several steps: supersaturation, nucleation, coagulation growth, and formation of polymer nanoparticles. The method is simple, fast, and highly reproducible. The nanoparticle colloid has good dispersion and is easy to be functionalized. It is a common method for preparing drug-loaded nanomaterials, but there are also defects such as fewer types of suitable polymers and difficult control of the particle growth process [67].

The microemulsion method is similar to the nanoprecipitation method. The prepared amphiphilic polymer and fluorescent material are first dissolved in a good solvent and then mixed with a poor solvent (usually deionized water) [68]. The huge difference in solubility is used to prepare nanoparticles, but the difference is that a certain concentration of surfactant needs to be added. However, the final surfactant is difficult to remove from the reaction system, which affects the application of fluorescent nanoparticles in the biological field. Additionally, the size of the prepared nanoparticles is relatively large, between 240 and 270 nm [69–71].

The usual preparation of the self-assembly method is to dissolve fluorescent materials and functional materials with opposite charges in an aqueous solution according to a certain ratio. After fully stirring and mixing evenly, the functionalized polymer nanoparticles are prepared using high-speed centrifugation and the particle size is about 100 nm. However, the preparation of the self-assembly method also has the instability of nanoparticles in a physiological environment, which limits its further application [72,73].

3.3. Preparation Method of Covalently Linked Fluorescent Polymer Nanoparticles

By means of covalent connection, fluorescent materials and amphiphilic block polymer materials are connected and self-assembled into polymer nanoparticles with luminescent properties, mainly including two types of nanoparticles: polymer micelles and nanogels.

3.3.1. Preparation of Polymer Micelles Using Aggregation-Induced Self-Assembly (PISA)

The traditional preparation methods of polymer micelles mainly include the solvent induction method, dialysis method, and direct dissolution method [74,75]. Nanoparticles with morphologies such as spherical, worm-like, and vesicular are prepared using the self-assembly of amphiphilic block polymers with different solubility differences in different solvents. However, the operation is complicated, the reaction takes a long time, and the concentration of the prepared nanoparticles is low (≤ 1 mg/mL), which makes it impossible to achieve large-scale mass production [76–78]. In recent years, the polymerization-induced self-assembly (PISA) method can not only prepare micelles and assemblies with different morphological structures (including spherical, worm-like, vesicular, etc.) in one pot, but nanoparticles with solids content up to 50% can also be synthesized in bulk [79,80]. This provides a new idea for the commercial application of preparing polymer nanoparticles, and is also widely used in the fields of drug-controlled release, bioimaging, and catalysis [81,82].

Hawkett et al. [83] first used polyacrylic acid (PAA) as a water-soluble macromolecular RAFT chain transfer agent and induced self-assembly into spherical micelles in aqueous solution. Subsequently, Pan et al. [84,85] utilized poly-4-vinylpyridine (P4VP) as a macromolecular RAFT chain transfer agent for dispersion polymerization in methanol solvent. With the chain growth of PS spheres, the morphology of the polymer gradually changed from spherical to worm-like and vesicle-like. A schematic diagram of nanomaterials prepared using the aggregation-induced self-assembly method [86] is shown in Figure 5. The water-soluble polymer chain transfer agent (macro-CTA) prepared using the RAFT method initiates another hydrophobic polymer monomer, and the newly synthesized diblock polymer can be dissolved in the reaction system at the early stage of the reaction. With the continuous growth of the second hydrophobic chain, the volume of the insoluble polymer continues to increase. When the critical micelle concentration (CMC) is reached, it self-assembles into different morphologies. A series of theoretical studies have shown that the morphology of block polymer self-assembly is determined by the volume ratio P of the polymer at the hydrophobic end. When $P \leq 1/3$, the diblock polymer exhibits

spherical nanoparticles. When $1/3 < P \leq 1/2$, the diblock polymer exhibits worm-shaped nanoparticles. When $1/2 < P \leq 1$, the diblock polymer exhibits a vesicle shape.

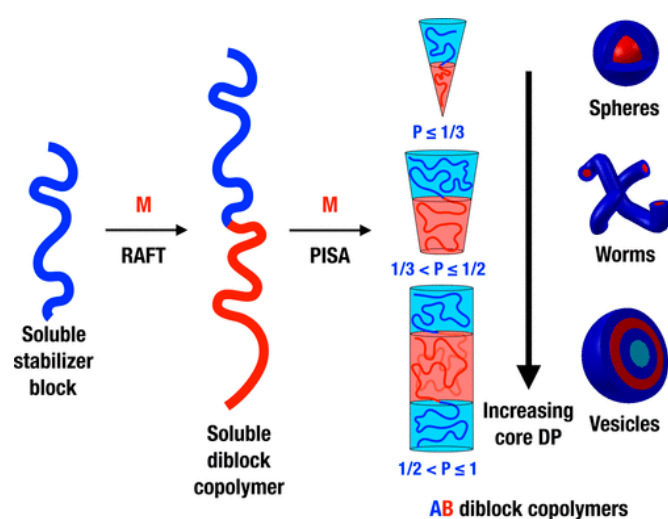


Figure 5. Schematic diagram of the preparation of nanoparticles from diblock polymers using the PISA method [86]. Copyright (2016), with permission from American Chemical Society.

3.3.2. Preparation of Nanogel Polymer Microspheres Using Precipitation Polymerization

Hydrogel is a kind of hydrophilic polymer material with a three-dimensional network structure, which can absorb water several times the weight of the material and has good biocompatibility and degradability [87]. Nanohydrogels are hydrogels with a size between 100 and 1000 nm that have the dual characteristics of hydrogels and nanomaterials. The structure is stable under physiological conditions, and it has a high drug loading rate and a long drug release cycle. It is a drug carrier material that has developed rapidly in recent years [88,89].

The nanogel preparation method [90] is shown in Figure 6. The traditional preparation methods mainly include emulsion polymerization, microemulsion polymerization and dispersion polymerization, all of which need to add stabilizers or surfactants to stabilize the reaction system and avoid aggregation and precipitation. However, it is difficult to remove the stabilizer or surfactant from the reaction system after the reaction, which affects the application of polymer microspheres in the biomedical field [91]. The method of precipitation polymerization was first proposed by Chibante et al. [92]. The stabilizer is replaced by a cross-linking agent, which is added to the reaction system together with the reactive monomer, and polymer microspheres with uniform particle size and clean surface are prepared after heating and polymerization. However, this method is only suitable for the polymerization of hydrophobic monomers and cannot prepare polymer microspheres for biomedicine. To expand the application of precipitation polymerization to hydrophilic monomers, Yang et al. [93] developed a distillation precipitation method, which shortened the precipitation polymerization time to 1–2 h. However, with the decrease in the solvent amount in the reaction system, the late reaction was unstable and the product yield was low. Wang et al. [94] developed the reflux precipitation polymerization method based on the technique of distillation precipitation. A return-shaped condenser was connected to the reaction device to ensure that the volume of the solvent in the reaction system remained unchanged, making the polymerization of the reaction system more stable. Compared with the traditional preparation method, the reflux precipitation polymerization method has the characteristics of short time consumption, no need for stabilizer, clean particle surface, simplicity of device, and less byproducts.

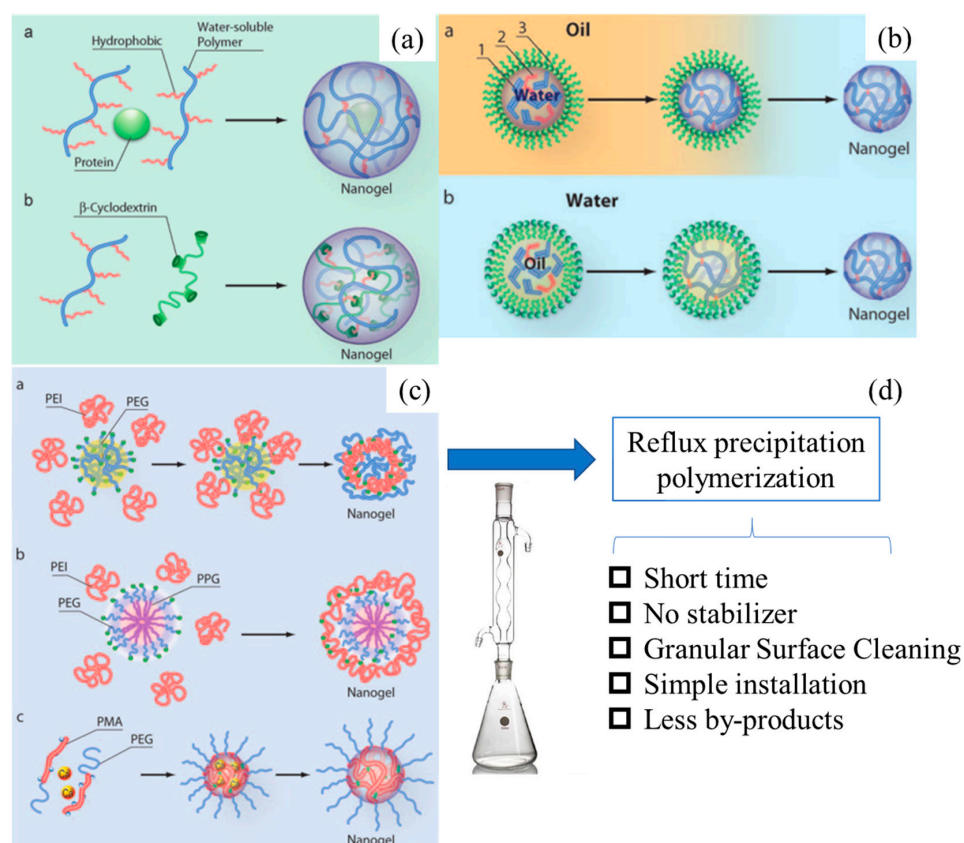


Figure 6. Schematic diagram of the nanohydrogel preparation method: (a) polymer self-assembly method; (b) inverse emulsion polymerization method; (c) precipitation polymerization method; (d) reflux precipitation polymerization method [90]. Copyright (2009), with permission from Wiley.

4. Biotoxicity of Fluorescent Polymer Nanomaterials

Due to their unique physical and chemical properties, nanomaterials have broad application prospects in the field of biomedicine. For example, as a drug carrier or a bioimaging probe, the pharmacokinetics and potential toxic effects in the organism need to be tested before practical application. *In vivo* toxicity studies of nanomaterials involve a variety of exposure methods, such as intravenous, transdermal absorption, subcutaneous, inhalation, intraperitoneal, and oral administration, and various animal models such as mice, rats, dogs, and monkeys. After nanomaterials enter the body and interact with biological components (proteins, cells), they are distributed to different organs of the body. At this point, the particles maintain their original structure or degrade. The slow removal and accumulation of materials, as well as the large number of phagocytes make the liver, spleen, and other organs in the reticuloendothelial system the most important targets of oxidative stress of nanomaterials. In addition, organs with high blood flow, such as lungs and kidneys, are also affected by nanomaterials [95].

Current toxicological mechanisms of nanomaterials mainly focus on the hypothesis of free radical oxidative damage [96]. This hypothesis holds that, under normal conditions, the content of reactive oxygen species in the mitochondria of body cells is very low. Additionally, there are many antioxidant systems in the body, and the active oxygen free radicals produced by normal cell metabolism are easily removed by glutathione reductase and antioxidant enzymes. When nanoparticles enter the body, they can induce the production of a large amount of reactive oxygen species (ROS). ROS mainly activate the inflammatory response by activating the phosphorylation of NF- κ B transcription factors and MAPKs. As a result, the antioxidant defense system in the mitochondria is destroyed, causing various damages and further affecting the normal physiological functions of the body.

Li et al. [97] found that nanoparticles can induce an increase in reactive oxygen species in RAW264.7 cells, leading to cell apoptosis. Shvedova et al. [98] summarized the main mechanism of nanoparticle-induced ROS generation in cells, resulting in oxidative damage: (1) oxidation of liposomes in mitochondria; (2) NADPH oxidation leading to cell apoptosis and inflammatory response; (3) depletion of reduced glutathione in the body; (4) activation of peroxidase, leading to degradation of nanoparticles. At the same time, this is precisely the oxidative damage effect of nanoparticles exposed to the body.

In addition to ROS, reactive nitrogen species (RNS) may also be involved in the free radical oxidative damage effect of nanoparticles. Recent studies have proved that RNS play a role in the inflammatory damage caused by nanoparticles. Lanone and Boczkowski suggested that the main molecular mechanism of *in vivo* toxicity of nanomaterials is the induction of free radicals leading to oxidative damage [99]. Free radicals can not only cause damage to biological components by oxidizing lipids, proteins, and DNA, but also induce and enhance inflammation by upregulating redox-sensitive transcription factors (such as NF- κ B) and inflammation-related kinases [100,101]. The composition of some materials, such as iron, cadmium, chromium, and other atoms also affects the toxicity *in vivo*. In addition, surface modification of nanoparticles can alter their interaction with cell membranes, resulting in their altered cellular uptake, thereby affecting their toxicological effects on targeted cells. The application and toxicity of different fluorescent nanomaterials in biological systems are shown in Table 2.

Table 2. Biotoxicity and biological system applications of different fluorescent nanomaterials.

Fluorescent Nanomaterial Type	Intrinsic Material Toxicity	Materials	Biological System
Carbon dots	Low	C-dots, PEG stabilized	Mice
Carbon nanotubes	Low–medium	Many types of CNTs	Various <i>in vitro</i> / <i>in vivo</i>
Dendrimers	High	Various dendrimer types	Various <i>in vitro</i> / <i>in vivo</i>
Doped graphene QDs	Medium	N-doped graphene quantum dots	Red blood cells
Fluorescent beads	Medium (polymer)	Polystyrene nanoparticles	Endothelial cells
Fluorescent proteins	Low (silica)	Silica nanoparticles	Epithelial cells and fibroblasts
	Medium	Red fluorescent protein	HeLa cells
Graphene oxide	Medium	Graphene oxide	Various <i>in vitro</i> / <i>in vivo</i>
Organic dyes	Medium	Graphene oxide	Red blood cells
Metal clusters	Medium	Various organic fluorophores	Various <i>in vitro</i> / <i>in vivo</i>
		MPA or GSH stabilized Au clusters	Colonic epithelial cells
		GSH and BSA stabilized Au ₂₅ clusters	Mice
Nanodiamonds	Low	Detonation nanodiamond	Various <i>in vitro</i> / <i>in vivo</i>
		Various diamond types	Human liver cancer and HeLa cells <i>in vitro</i>
		Detonation nanodiamond	Human embryonic kidney cells and <i>Xenopus laevis</i> embryos
P-dots	Medium	Quinoxaline based polymer, STV conjugated	Zebrafish embryo
		Polybutylcyanoacrylate	HeLa and human embryonic kidney cells/rats
Quantum dots	High	CdSe–ZnS; PEG, BSA or polymer stabilized CdTe	Rats
		Several types	Mice
		Several types	Various <i>in vitro</i> / <i>in vivo</i>
Rare earth nanoparticles	Medium-high	UCNPs, NaYF ₄ :Yb,Tm, polyacrylic acid coated	Various <i>in vitro</i> / <i>in vivo</i>
		UCNPs, NaYF ₄ :Yb,Tm	Mice
		DCNPs, Gd ₂ O ₂ S:Tb ³⁺	HeLa cells, <i>Caenorhabditis elegans</i> Human peripheral blood mononuclear cells, human-derived macrophages, HeLa cells

Because of the small size effect of nanomaterials and the complexity of biological systems, the effects caused by the processing of nanomaterials in biological systems are unpredictable. The interaction between biological components (proteins and cells) and nanostructured materials may cause unique biodistribution and metabolic reactions, making it difficult to predict the metabolism and safety of nanomaterials in biological systems. As evidenced by the above literature review, fluorescent materials have been widely used in biomedical fields such as bioimaging, biosensors, and drug delivery because of their excellent luminescent properties and photoconversion properties. However, due to their particularity, their biological safety cannot be predicted. Therefore, they may cause certain harm to organisms during use, which greatly limits the application of fluorescent nanomaterials. Therefore, it is urgent to find fluorescent nanomaterials with good biocompatibility.

5. Application of Fluorescent Polymer Nanomaterials in Bioimaging

In order to meet the needs of different biological applications, many different types of fluorescent polymer nanomaterials have been developed. This paper focuses on the research direction and focuses on the introduction of polymer nanomaterials based on rare earth luminescent materials, semiconducting polymers, and organic, small molecule luminescent materials [7–9]. The use of nano-fluorescent probes can quickly, accurately, and selectively label and study target molecules on cells. Labels were obtained according to their excitation wavelengths at different emission wavelengths, as shown in Table 3.

Table 3. Common fluorescence excitation and emission wavelengths.

Fluorescent Substance	Excitation Wavelength		Emission Wavelength EM nm
	EX nm	EX (sub)	
Alexa Fluor 532	532		554
Cy3	550		570
DsRed	557		579
EtBr	300	518	605
FITC	490		525
Gel Green	250	500	530
GFP	488		507
mCherry	580		610
SYBR Gold	495		540
SYBR Green I	498		522
SYPRO Red	550	300	630
SYPRO Ruby	280	450	620
TagRFP	555		583
Gel Red	270	510	600

5.1. Polymer Nanomaterials Based on Rare Earth Luminescent Materials

Rare earth elements include lanthanides with atomic numbers 57–71 in the periodic table of chemical elements and scandium (Sc, 21) and yttrium (Y, 39) with similar chemical properties, a total of 17 elements [102]. The electron configuration of lanthanides is $[\text{Xe}]4f^{0-14}5d^{0-16}s^2$, and each element has a 4f electron shell. Compared with other luminescent materials, it has narrow emission band (10–20 nm), high luminous efficiency, large Stokes shift, and long emission lifetime (range μs –ms) features [103]. At present, rare earth luminescent materials used in biological imaging mainly include rare earth organic complexes and rare earth upconversion materials.

5.1.1. Rare Earth Organic Complexes

Rare earth organic complexes are due to the small molar absorptivity of lanthanide trivalent ions and the prohibition of ff transitions in the electron shell [104,105]. As a result, very little energy is directly absorbed by the 4f energy level of lanthanide elements, and organic ligands are required to act as antennas to absorb excitation energy, thereby sensitizing rare earth ions to emit light. This process is called “antenna” (Figure 7a) [106].

As shown in Figure 7b, the main process of energy transfer of rare earth complexes is as follows: (1) After the rare earth complex absorbs energy, electrons transition from the ground state (S_0) to the excited state (S_1). (2) The energy of the excited state (S_1) transfers energy to the lowest excited triplet state (T_1) through intersystem crossing (ISC). (3) When the lowest excited triplet state (T_1) matches the lowest excited state energy level (5D_J) of rare earth ions, energy transfer occurs between T_1 and 5D_J . Eventually, the rare earth ions return to the ground state (7F_J) in the form of radiation, thereby emitting the characteristic fluorescence of rare earth ions [103,107,108].

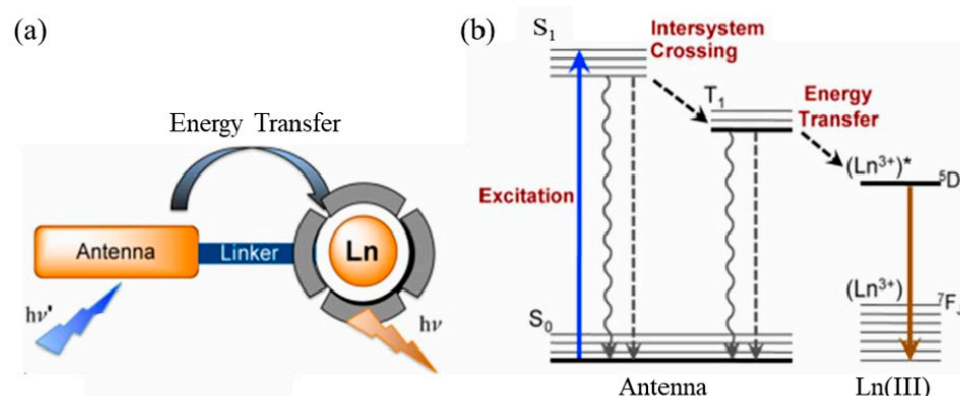


Figure 7. (a) Schematic diagram of the antenna effect of rare earth complexes; (b) schematic diagram of the luminescent principle of rare earth complexes [103]. Copyright (2014), with permission from American Chemical Society.

According to the structure of the ligands, it can be divided into β -diketone ligands, carboxylic acid ligands and macrocyclic ligands such as crown ethers [109]. There are coordination elements such as O, N, and S on the ligand, and a stable six-membered ring structure is formed after coordination with rare earth. It can directly absorb laser energy and effectively transfer energy to rare earth ions through the structure of the six-membered ring, and then emit the characteristic fluorescence of rare earth ions. The coordination ability of the coordinating atoms is $O > N > S$. When rare earth complexes are used in biological imaging, water molecules easily replace the coordination bonds of organic ligands [110]. The high-frequency O–H bonds of water increase the nonradiative decay of excited states of rare earth ions, which in turn affects the luminescent properties of rare earths [111]. When rare earth organic complexes are used as fluorescent probes, they are usually physically wrapped with biocompatible silica or polyethylene glycol to form a core–shell structure, which improves the chemical stability of the material and avoids the interference of water molecules.

Dos Santos et al. used the polymer PMMA-COOH to physically wrap the rare earth complex $\text{Eu}(\text{TTA})_3\text{phen}$, and the preparation's schematic diagram is shown in Figure 8. By adjusting the concentration of the precursor, rare earth polymer nanoparticles of 10 nm, 20 nm, and 30 nm were prepared. The fluorescence quantum efficiency exceeded 20%, and the brightness of a single particle was as high as $4.0 \times 10^7 \text{ M}^{-1} \text{ cm}^{-1}$. A lower laser intensity of 0.24 W/cm^2 can be used to image single particles, and time-resolved imaging microscopy can be used to dynamically observe the progress of nanoparticles into cells [112]. However, the polymer physically wraps the rare earth complex material, and there is also uneven distribution of the fluorescent material. Aggregation quenching is prone to occur, which affects the luminescent properties of fluorescent probes, and the related preparation methods still need further research [113–115].

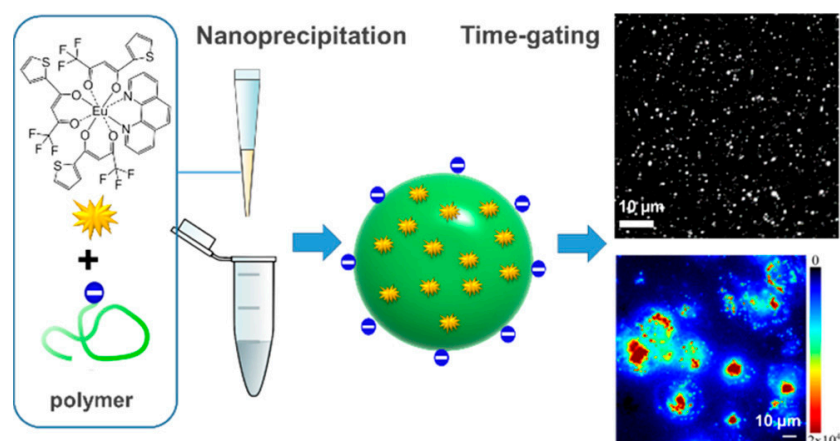


Figure 8. Schematic diagram of rare earth polymer nanoprobe for single particle detection and cell imaging [112]. Copyright (2019), with permission from American Chemical Society.

In order to solve the problem of uneven distribution of fluorescent materials in polymer nanosystems, Xu et al. [116,117] modified hydroxyl and amino groups on $\text{Eu}(\text{TTA})_3\text{phen}$, respectively. As shown in Figures 9a and 10, two complexes, $[\text{Eu}(\text{TTA})_3\text{phen}]\text{-OH}$ and $(\text{Eu}(\text{TTA})_3\text{phen})\text{-NH}_2$, were prepared. They then reacted with hydrophilic polymers PEG2000 and GluEG NCA through covalent connection to generate $[\text{Eu}(\text{TTA})_3\text{phen}]\text{-PEG2000}$ and $[\text{Eu}(\text{TTA})_3\text{phen}]\text{-GluEG}$, respectively, and self-assembled into water-soluble nanoparticles. They emit the 614 nm characteristic peak of Eu(III) ion in aqueous solution, and can be successfully taken up by L929 cells and HeLa cells, and emit strong red light (as shown in Figures 9b and 10).

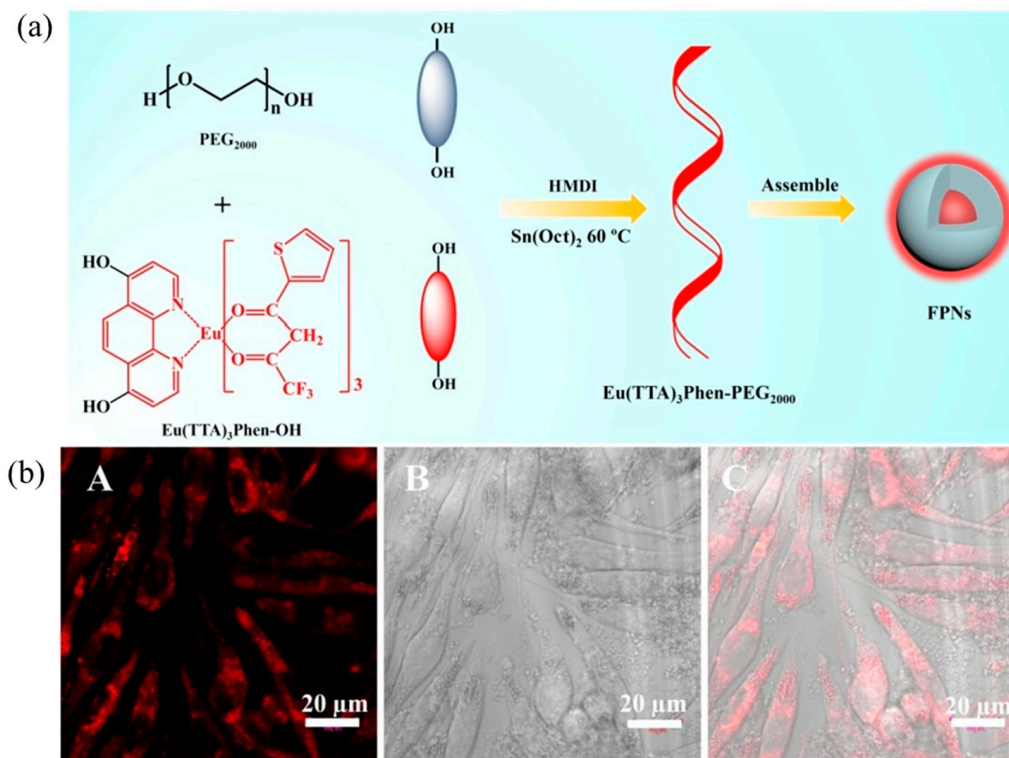


Figure 9. $[\text{Eu}(\text{TTA})_3\text{phen}]\text{-PEG2000}$ nanomaterials: (a) schematic diagram of preparation; (b) cell imaging diagram. (A) fluorescent image 405 nm laser excitation, (B) bright field and (C) merged image of (A,B). Scale bar $\frac{1}{4}$ 20 mm. [116]. Copyright (2018), with permission from Elsevier.

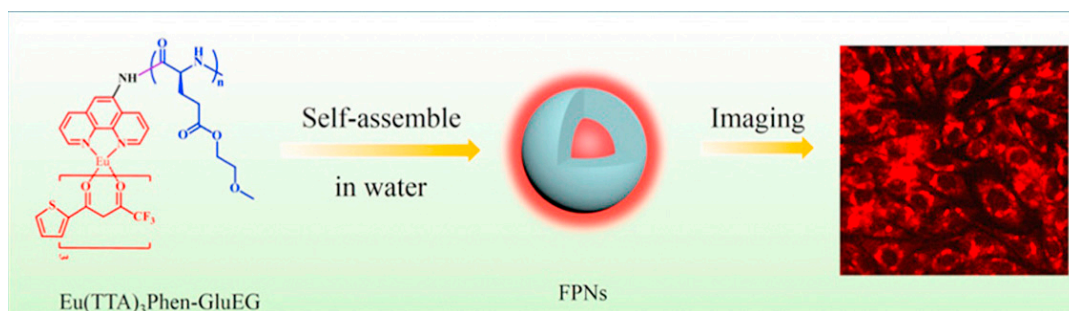


Figure 10. Preparation and cell imaging of [Eu(TTA)₃phen]-GluEG nanomaterials [117]. Copyright (2018), with permission from Elsevier.

5.1.2. Rare Earth-Doped Upconversion Luminescent Materials

Rare earth-doped upconversion materials are doped with trivalent lanthanide ions into a suitable dielectric matrix lattice. The lanthanide ions act as the luminescent center, and the ground state electrons of the sensitized ions are first excited to the excited state under the irradiation of the excitation light of a suitable wavelength. Then, the energy is transferred to the luminescent center, and the luminescent center is excited to an excited state. Finally, the excited state electrons return to the ground state and emit near-infrared fluorescence. Therefore, sensitizing ions are required to have a larger absorption cross-section at NIR-I or NIR-II. For example, the luminescent central ions with NIR-I emission include Nd³⁺, Yb³⁺, and Er³⁺, and the luminescent central ions with NIR-II emission include Nd³⁺, Ho³⁺, Pr³⁺, Tm³⁺, and Er³⁺ (as shown in Figure 11) [118]. Rare-earth-doped upconversion materials have the advantages of low toxicity, narrow-band emission, long emission lifetime, no photobleaching, and no scintillation. They have broad application prospects in the fields of bioimaging, such as in analytical sensors, PDT, and optical imaging [119].

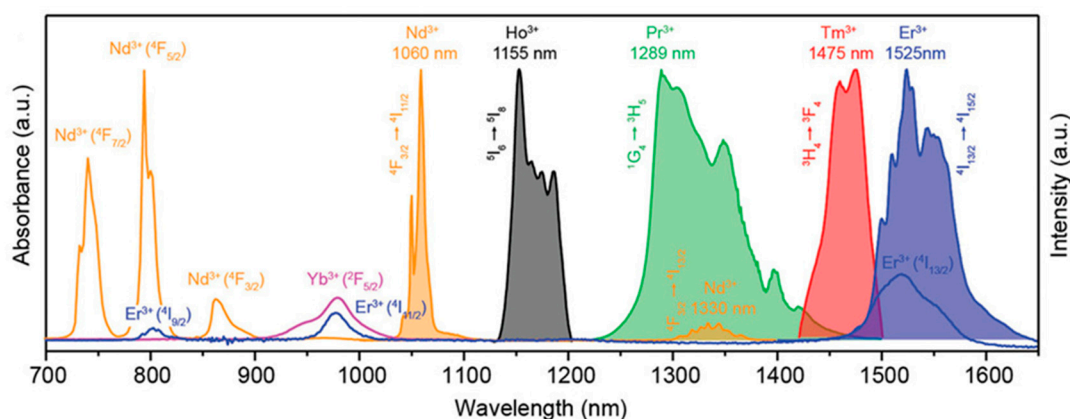


Figure 11. Absorption spectra of Nd³⁺, Er³⁺, and Yb³⁺ in NIR-I and emission spectra of Nd³⁺, Ho³⁺, Pr³⁺, Tm³⁺, and Er³⁺ in NIR-II [118]. Copyright (2019), with permission from Wiley.

Rare earth-doped upconversion luminescent materials are generally hydrophobic. Generally, water-soluble bioluminescent probes are prepared by modifying the surface function of materials with SiO₂ that has better biocompatibility, water-soluble polymers (PEG, PAA, PEI, etc.), and polyols. Tao et al. [120] used the block polymer PEO-b-PCL to wrap NIR-I emitting rare earth nanocrystalline materials NaYF₄:Yb/Ho(DiR) and NIR-II-emitting NaCeF₄:Er/Yb(LNPs). And luciferase (LUS) and red fluorescent protein (RFP) were doped into the polymer to prepare a multifunctional nanomaterial that can simultaneously generate NIR-I and NIR-II fluorescence spectra (as shown in Figure 12a–c). Then, the nanomaterials were injected intraperitoneally into mice with ovarian cancer, and fluorescence signals of two spectra could be found in the ovarian LUS+/RFP+-responsive cancer cell OVCAR-8 (Figure 12d).

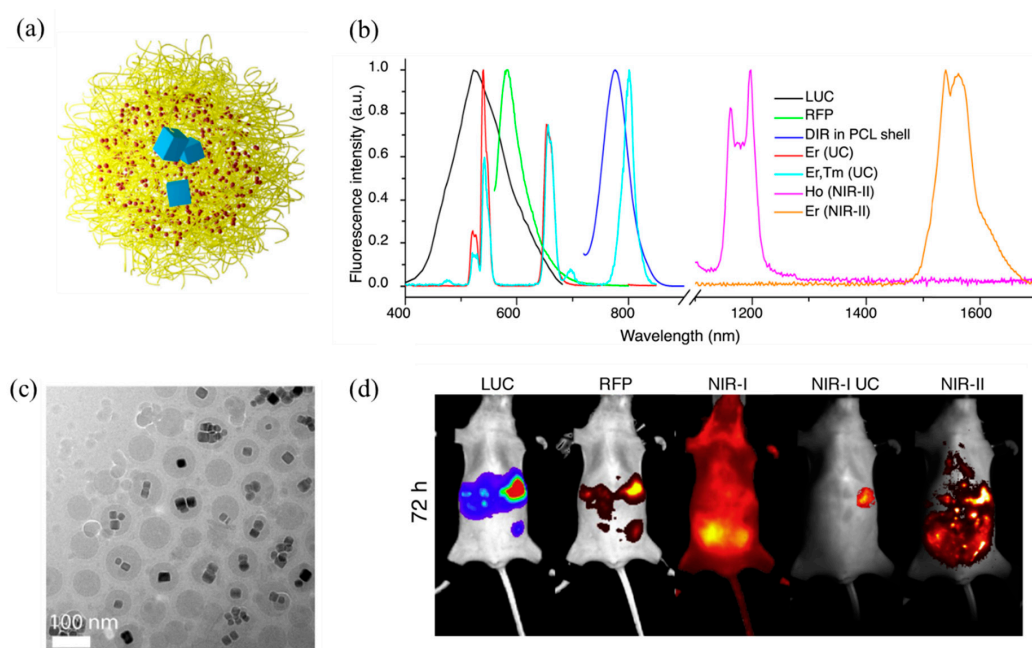


Figure 12. (a) Schematic diagram of nanoparticles, in which the yellow block represents the block polymer PEO-*b*-PCL, the red point represents the NIR-I quantum dot DiR, and the blue block represents the NIR-II quantum dot LNPs; (b) the nanoparticle TEM image; (c) fluorescence spectrum of multifunctional nanomaterials; (d) imaging of multifunctional nanoparticles in mice [120]. Copyright (2017), with permission from Elsevier.

5.2. Polymer Nanomaterials Based on Semiconducting Polymers

Semiconductor polymers (SPs) are a class of polymer materials whose main chain is composed of π - π -conjugated structures [121,122]. Due to the excellent optoelectronic properties and good processing properties of semiconductors, they were first applied in the field of organic optoelectronics. At present, semiconducting polymer materials commonly used in the biomedical field are divided into polyfluorene (PF), polythiophene (PT), poly(phenylene ethylene, PPE) and poly(p-phenylene vinylene, PPV) according to the structure of the main chain. Their derivatives [123,124] and structure are shown in Figure 13.

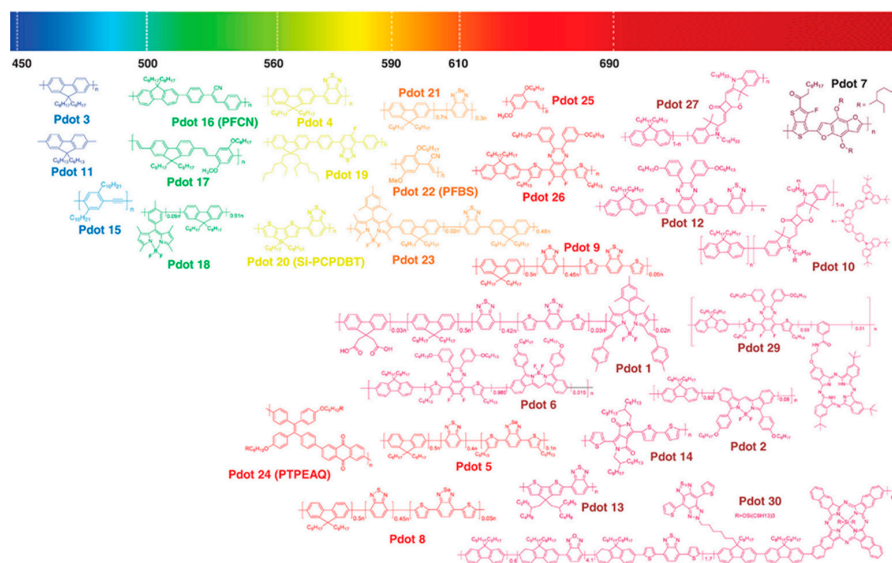


Figure 13. Chemical structures of semiconducting polymers [125]. Copyright (2019), with permission from Wiley.

From the perspective of the main chain structure of the semiconducting polymer, it is a typical rigid structure and hydrophobic, and aggregation occurs in aqueous solution, resulting in fluorescence quenching. At present, the commonly used method is to directly physically encapsulate semiconducting polymer materials in amphiphilic block polymers to prepare water-soluble polymer fluorescent nanoparticles (SPNs). Not only can this effectively solve the problem of monodispersion of semiconducting polymers in water, but the surface can also be easily functionalized. They have been widely used in the fields of tumor diagnosis [126–128] and antibacterials [129–131]. Among them [15], polyethylene glycol (PEG) is widely used to modify semiconducting polymers because of its characteristics of increasing drug solubility, reducing body immunity, and prolonging the residence time of drugs in the body [132].

In order to improve the fluorescence quantum efficiency of semiconducting polymers, Fan et al. used low-energy-band ester-based semiconducting polymers to skillfully control intramolecular charge transfer (ICT) to increase the intensity of NIR-II fluorescence [133]. As shown in Figure 14, as the thiophene group chain lengthened (TT-T to TT-3T), the ICT gradually weakened, and the corresponding NIR-II fluorescence emission gradually increased. TT-3T CPs (51–70 nm) were prepared by physically wrapping TT-3T with amphiphilic block polymer F127. They emit NIR-II light (1050 nm) in aqueous solution with a fluorescence quantum efficiency of 1.75%. Moreover, in vivo cell tracking, vascular system imaging, and lymphatic drainage mapping all had good imaging effects and high NIR-II spatial resolution.

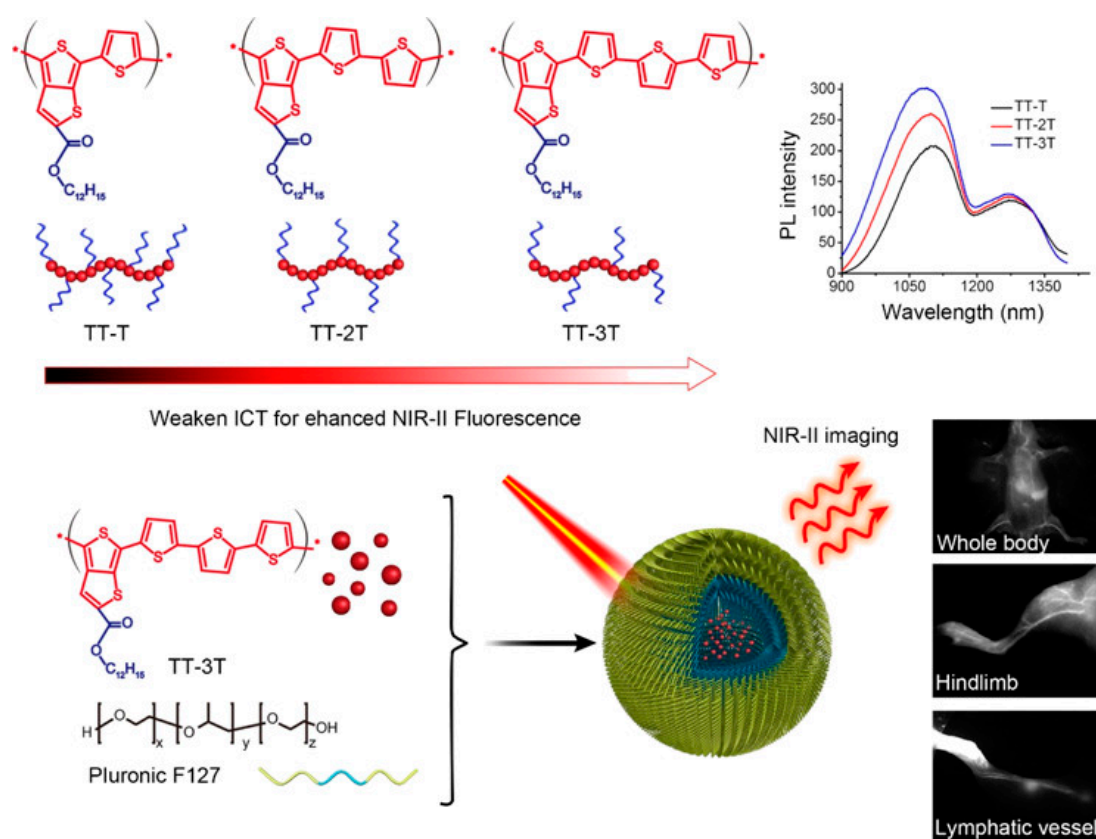


Figure 14. Schematic diagram of the synthesis of ester-based semiconducting polymer TT-3T CPs and their application in bioimaging [133]. Copyright (2019), with permission from American Chemical Society.

In order to further study the NIR-II real-time imaging application of semiconducting polymers in vivo, Hong et al. [134] designed and synthesized a NIR-II semiconducting polymer pDA (Figure 15a). After being physically encapsulated with the amphiphilic block polymer DSPE-MPEG (5kDa), pDA-PEG nanoparticles with a particle size of 2.9 nm

were prepared (as shown in Figure 15b,c). The fluorescence emission wavelength is about 1000 nm (Figure 15d), the fluorescence quantum efficiency is about 1.7%, and it has been successfully applied to real-time imaging of vascular diseases.

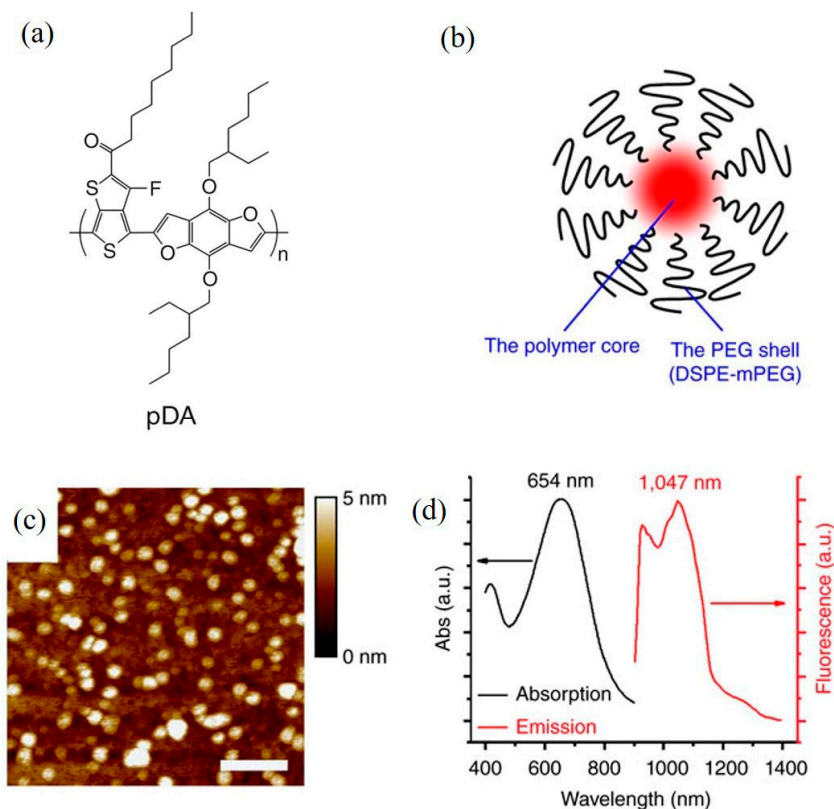


Figure 15. (a) Molecular structure diagram of semiconducting polymer pDA; (b) schematic diagram of pDA-PEG nanoparticles; (c) AFM image of pDA-PEG nanoparticles; (d) absorption and emission diagram of pDA-PEG nanoparticles aqueous solution [134]. Copyright (2014), with permission from Springer Nature.

Some semiconducting polymers are prone to the aggregation-caused quenching (ACQ) phenomenon after they are prepared into nanoparticles using physical encapsulation of amphiphilic block polymers [135,136]. Zhang et al. [137] used phenothiazine, which has typical AIE characteristics, as the electron donor. As shown in Figure 16a, different groups were introduced into the side chains to compare the effect of weakening ACQ. The study found that the emission wavelength of P3c modified with 9,10-diphenylanthracene (9,10-diphenylanthracene) was larger than that of P3a modified with hexane, and the emission intensity was high. Then the polymers P3a and P3c were physically encapsulated using the amphiphilic block polymer PS-PEG to prepare P3a NPs and P3c NPs, which were injected into mice. As shown in Figure 16b,c, the mice in the P3c NPs group glowed red, while the mice in the P3a NPs group did not. Additionally, because P3c NPs have strong NIR-II luminescent properties, the skull and cerebral blood vessels of mice can be clearly observed when performing imaging in mice.

Fluorescence brightness is determined using the absorption cross-section and the fluorescence quantum efficiency. Fluorescence quantum efficiency refers to the ratio of the number of emitted photons to the number of absorbed photons, which is one of the important parameters for evaluating the performance of fluorescent probes. The emission wavelength range of polymer quantum dot PFBT is comparable to that of Qdot 565, a commonly used fluorescent probe, inorganic semiconductor quantum dot, and IgG-Alexa 488, which contains approximately six dye molecules per IgG antibody. Therefore, the photo-physical properties of the three are summarized and compared (see Table 4).

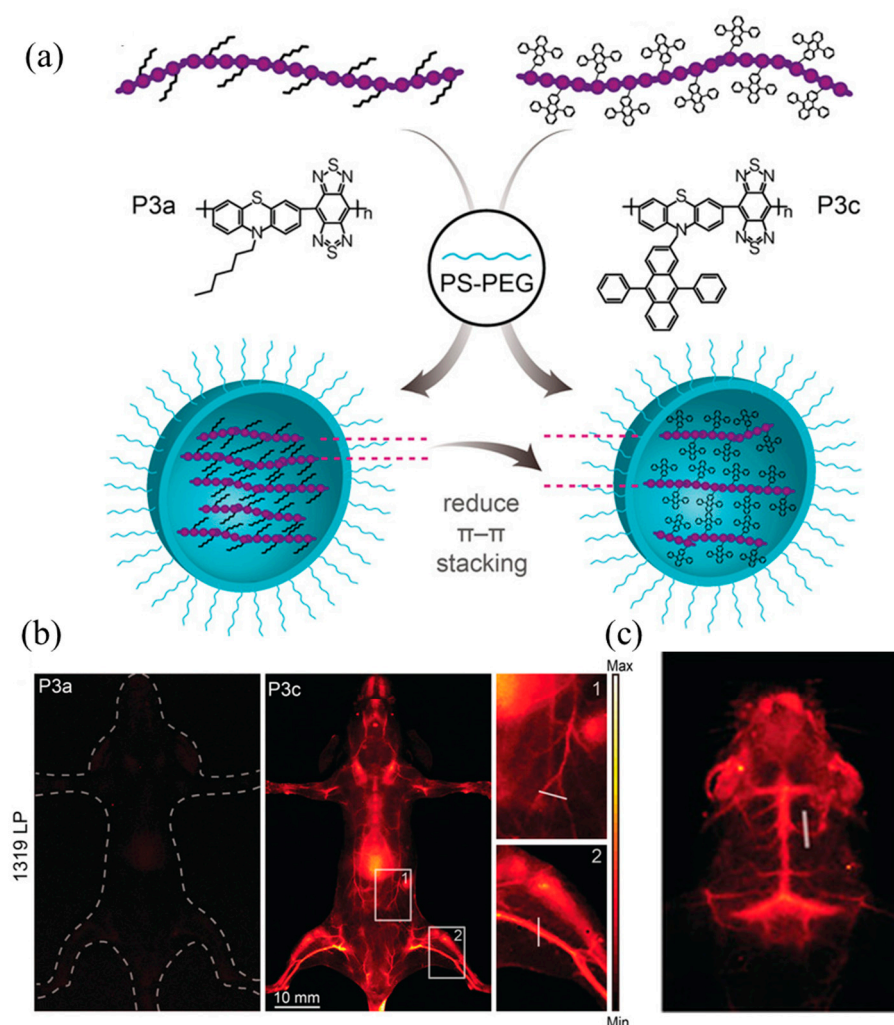


Figure 16. (a) Schematic diagram of the preparation of P3a NPs and P3c NPs; (b) NIR-II images of mice injected with P3a NPs and P3c NPs, respectively; (c) vascular NIR-II images of skull and brain of mice injected with P3c NPs [137]. Copyright (2020), with permission from Wiley.

Table 4. Several photophysical properties of PFBT Pdots, IgG-Alexa 488, and Qdot 565 [138].

Probes Size	PFBT ~10 nm	IgG-Alexa 488 ~1 nm	Qdot 565 ~15 nm
Abs/FL λ_{\max} (nm)	460/540	496/519	UV/565
ϵ ($M^{-1}cm^{-1}$) $\lambda = 488$ nm	1.0×10^7	5.3×10^4	2.9×10^5
Quantum yield (%)	30	90	30~50
Fluorescence lifetime (ns)	0.6	4.2	~20

It can be seen from Table 1 that, when the three nanoparticles are excited by a laser with a wavelength of 488 nm, the single-particle luminescence brightness of PFBT quantum dots with a size of about 10 nm is about 30 times higher than that of IgG-Alexa 488 and Qdot 565. At a wavelength of 488 nm, the absorption cross-section of PFBT quantum dots is approximately half of its own peak absorption cross-section. The luminescence brightness of the three fluorescent probes was compared in parallel using single-particle imaging experiments [139]. Experiments have found that when the probe is excited by a laser with a wavelength of 488 nm, when the excitation power is low, a single PFBT nanoparticle with high luminescence brightness close to the diffraction limit can be observed. Under the same conditions, the luminescence of IgG-Alexa 488 and Qdot 565 probes was found to be very weak. The camera used in the experiment barely captured the fluorescent signal. After counting the fluorescence intensity distribution of thousands of nanoparticles, it was

found that the luminescence brightness of PFBT nanoparticles was about 30 times higher than that of IgG-Alexa 488 and Qdot 565 probes. These experimental data are consistent with the results based on the comparison of photophysical parameters.

5.3. Polymer Nanomaterials Based on Organic Fluorescent Small Molecules

The luminescence intensity of fluorescent probes determines the signal-to-noise ratio and imaging depth of the probes. If polymer nanoparticles with higher brightness are to be prepared, more fluorescent materials need to be encapsulated into the polymer nanoparticles. However, in most fluorescent probe materials, as the concentration increases, the fluorescence aggregation-induced quenching (ACQ) phenomenon occurs [140,141]. Tang et al. [142] first proposed the aggregation-induced emission (AIE) phenomenon, and AIE materials are an effective way of solving the above problems. Qi et al. [143] designed and synthesized the AIE compound TQ-BPN, and prepared TQ-BPN nanoparticles with a particle size of 33 nm after physical wrapping with the amphiphilic block polymer Pluronic F-127 (as shown in Figure 17a). The fluorescent quantum effect was as high as 13.9%. Although the maximum emission wavelength was in the NIR-I region (808 nm), there was still a fluorescence quantum efficiency of 2.8% in the NIR-II region (Figure 17b). Additionally, when TQ-BPN nanoparticles were used as fluorescent probes to perform fluorescence imaging on a mouse's brain, it was found that the imaging spatial resolution reached 2.6 μm and the penetration depth reached 150 μm . More importantly, as shown in Figure 17c, clearly identifiable fluorescent signals can be seen at various stages of tumor growth, which can be applied to early diagnosis of cancer. According to the mechanism of aggregation-induced luminescence, more and more AIE molecules have been designed and synthesized by researchers. Typical AIE small molecules include hydrocarbon molecules (1–3 molecules) and heterocyclic small molecules (4–9 molecules) (see Figure 18).

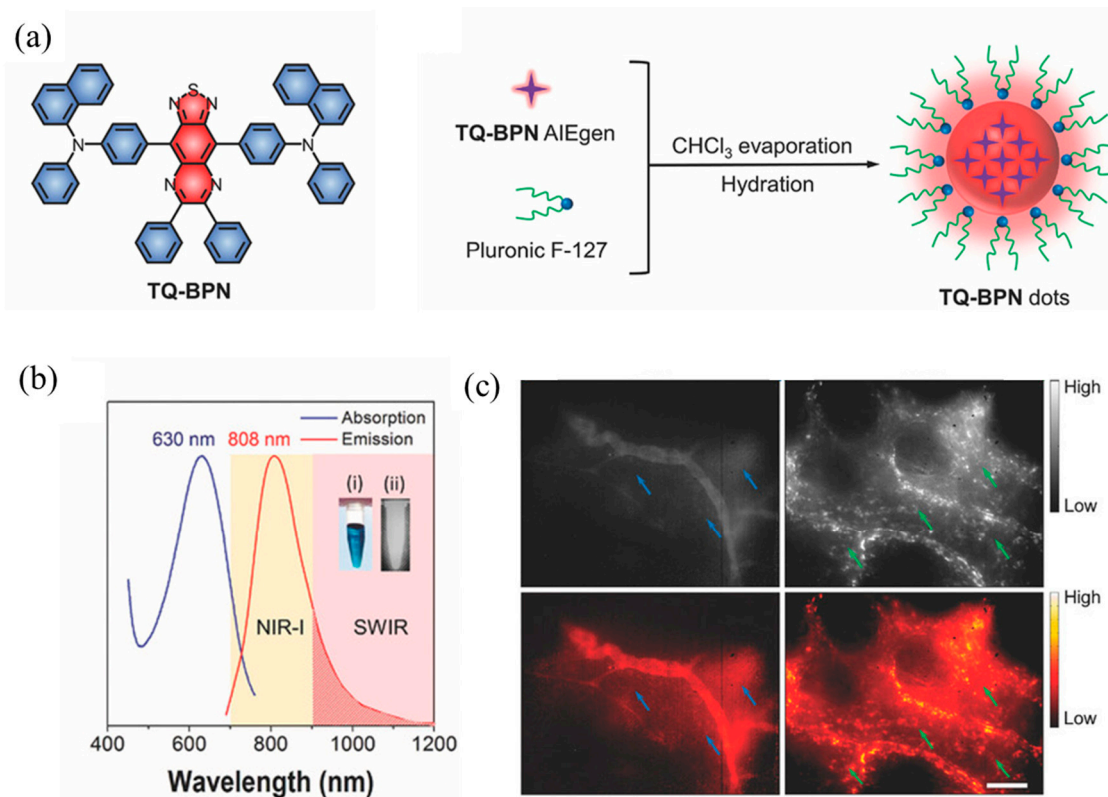


Figure 17. (a) Schematic diagram of TQ-BPN dot preparation; (b) TQ-BPN dot absorption and generation curves in aqueous dispersion; (c) NIR-II of TQ-BPN dots at different stages of tumor growth imaging [143]. Copyright (2018), with permission from Wiley.

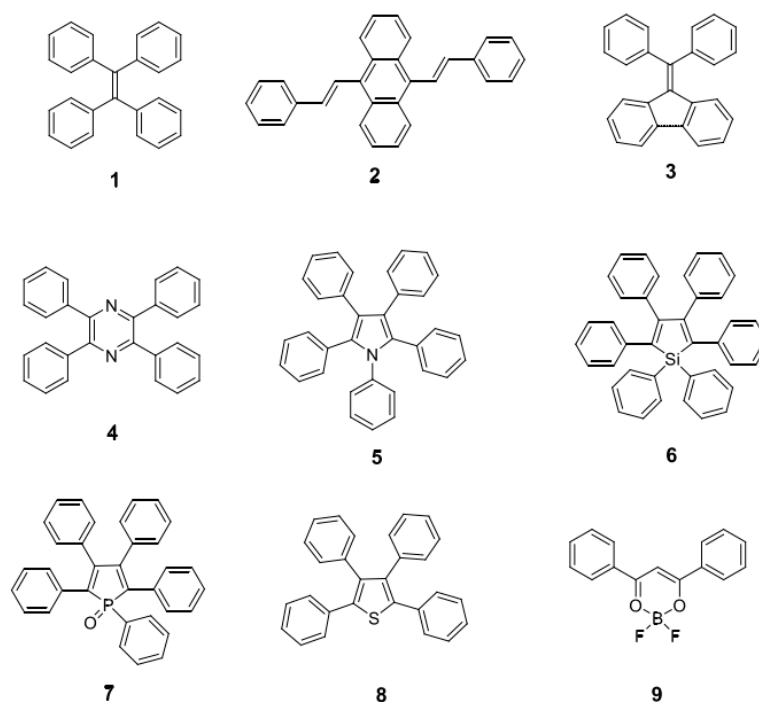


Figure 18. Typical AIE small molecules and their structures. 1. Tetraphenylethene (TPE); 2. Triphenylamine (TPA); 3. Phenothiazine (PTZ); 4. Benzothiazole (BTH); 5. 2-(2'-Hydroxyphenyl)benzoxazole (HBO); 6. 2-(4'-Biphenyl)-5-(4''-tert-butylphenyl)-1,3,4-oxadiazole (BBD); 7. 1,2,3,4,5-pentaphenylsilole (PPS); 8. 1,2-bis(4'-phenylvinyl)benzene (DPVBi); 9. 1,4-bis(2,2-diphenylvinyl)benzene (DPVBi-Ph).

In order to further improve the fluorescence efficiency of fluorescent probes in NIR-II, Sheng et al. [144] designed and synthesized a new AIE material, TB-1, containing a DA structure. TB-1 dots with a particle size of 32 nm were prepared after physical encapsulation using DSPE-PEG2000, and the schematic diagram of the preparation is shown in Figure 19a. The maximum emission wavelength of the nanomaterial exceeded 1000 nm in the aqueous dispersion system, and the fluorescence efficiency was as high as 6.2%. The blood vessels in the brain of the mouse could be clearly seen without opening the mouse's cranium. In addition, the targeting group c-RGD was further modified to the surface of nanoparticles using a Michael addition reaction, prepared into TB1-RGD dots, and then injected into mice, respectively. From the comparison of Figure 19b,c, it can be seen that the TB1-RGD dot group modified with the targeting group has obvious imaging in the tumor part of the mouse at 24 h. The corresponding TB-1 dots with unmodified targeting groups had no obvious imaging effect.

Although the AIE material is wrapped in the polymer model using physical wrapping, the monodispersity and biocompatibility of the water system of the AIE material improve. However, there are also nanomaterials prepared using physical encapsulation in different batches, showing different particle sizes and encapsulation effects. To prepare AIE nanomaterials with good uniformity, Li et al. [145] alkynylated the AIE material TTB-OH. As shown in Figure 20a, amphiphilic polymers were prepared using amino-alkyne click polymerization with the amino-modified hydrophilic PEG polymer PEG-NH₂, which then self-assembled into SA-TTB NPs. At the same time, as a comparison, as shown in Figure 20b, NDP-TTB NPs were prepared by directly encapsulating TTB-OH with the amphiphilic block polymer DSPE-PEG2000. From the TEM comparison images of nanoparticles in Figure 20c III, it can be seen that the two SA-TTB NPs prepared using the self-assembly method are more uniform in particle size and better in monodispersity than the NDP-TTB NPs prepared using the physical encapsulation method. By dispersing the three kinds of nanoparticles into the water system, it was measured that their maximum emission wavelengths were all around 1050 nm, with little difference. However, the fluorescence

efficiency of SA-TTB NPs in the water system was as high as 10.3%, which is much higher than that of physically encapsulated NDP-TTB NPs. Additionally, a resolution of 38 μm and a penetration depth of 1 cm can be achieved in mice.

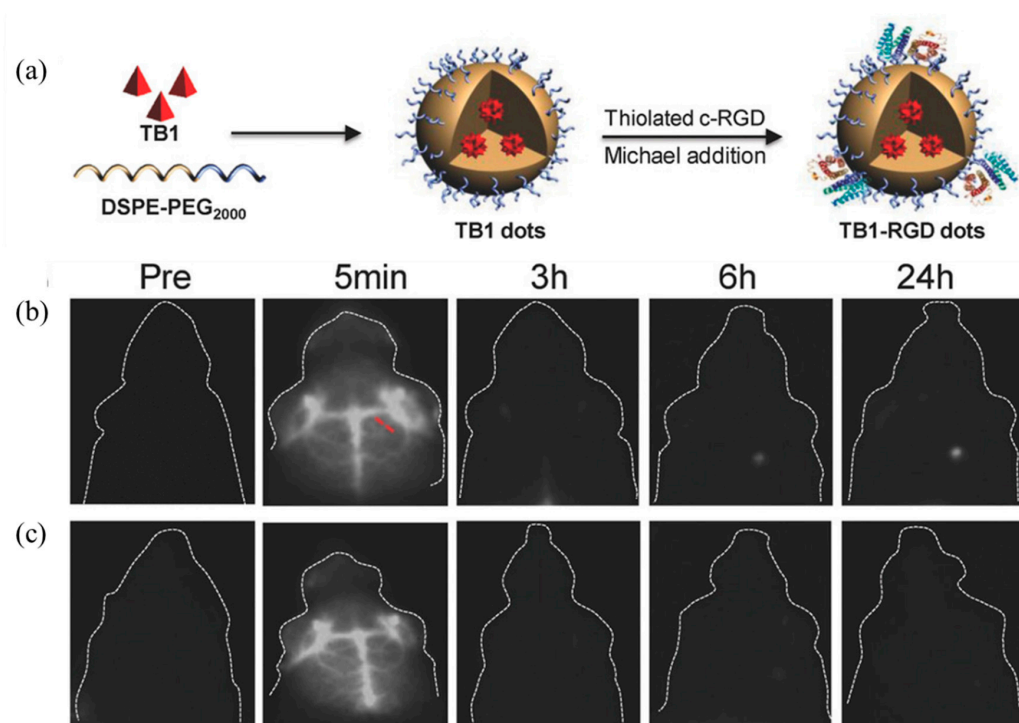


Figure 19. (a) Schematic diagram of the preparation of TB-1 dots and TB-RGD dots.; (b) imaging of TB-RGD dots injected into mice at different times. The red dashed line indicates the location of the intercepted area for calculating intensity of luminescence; (c) images of different time intervals of TB-1 dots injected into mice [144]. Copyright (2018), with permission from Wiley.

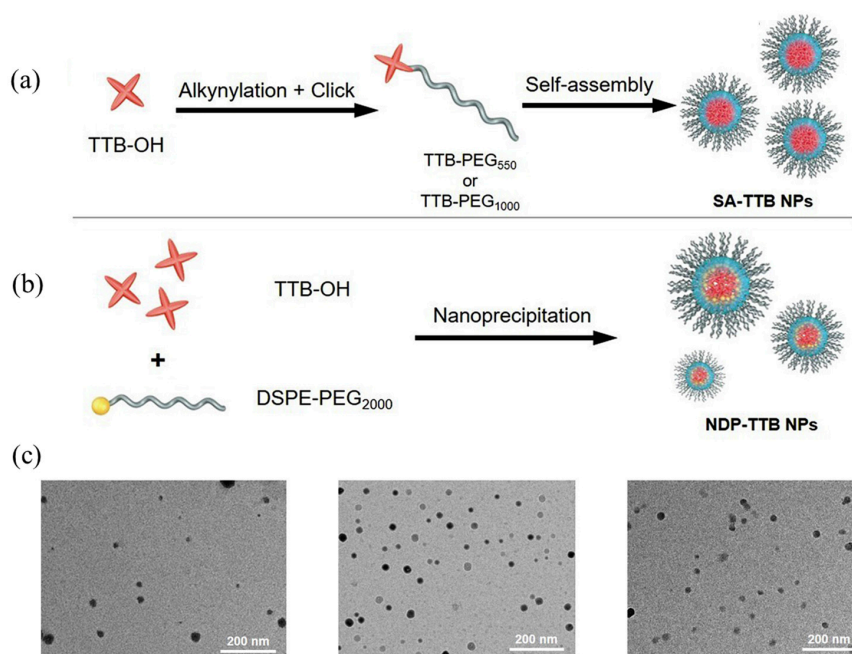


Figure 20. (a) Schematic diagram of TTB-OH self-assembly to prepare nanoparticles; (b) TTB-OH physical encapsulation method to prepare nanoparticles; (c) TEM images of three kinds of nanoparticles [145]. Copyright (2021), with permission from Elsevier.

In addition, based on the typical donor–acceptor–donor (D–A–D) structure, benzo-bisthiadiazole (BBTD) derivatives are representative organic small molecules [146,147]. With good biocompatibility, low biotoxicity, easy functionalization, and excellent metabolic ability, they show potential application prospects in the field of tumor imaging and treatment. However, BBTD-like derivatives are inherently hydrophobic and have no tumor-targeting ability. Polyethylene glycol (PEG) is often used for functional modification to prepare fluorescent polymer nanoprobe. Targeting groups are then attached to the surface of nanomaterials, so as to achieve partial targeted imaging of tumors and rapid metabolic clearance from organs such as the kidney or liver [148–150]. Dai et al. first used BBTD as the acceptor and triphenylamine (TPA) as the donor to prepare the compound CH1055 with a typical D–A–D structure. CH1055-PEG was prepared after modification with polyethylene glycol (PEG), and its maximum emission wavelength in water was 1055 nm. Experiments have shown that the imaging effect on mouse blood vessels and lymph is better than that of the commercial dye indocyanine green ICG, and about 90% of the material can be metabolically cleared from the kidney within 24 h [151]. In recent years, based on the compound CH1055, it has become possible to prepare a series of CH1055 derivatives by using different group modifications, such as the water-soluble CH-4T [152] prepared using sulfonation modification. With the help of follicle-stimulating hormone (FSH) modification, it is prepared into FSH-CH [153] and so on.

6. Summary and Outlook

Early diagnosis and treatment of cancer can greatly reduce its incidence and mortality. As a noninvasive and visualized diagnosis and treatment method, bioluminescence imaging technology, combined with traditional imaging technology, provides reliable imaging means for the early diagnosis of cancer. This article systematically introduces the research and development status and application prospects of fluorescent polymer nanomaterials based on rare earth luminescent materials, semiconducting polymers, and small organic molecules from recent years. Various types of luminescent probes have been developed for tumor diagnosis. However, due to the hydrophobic nature of the luminescent probe itself, when it is further functionalized, most of the luminescent materials are encapsulated inside the polymer nanoparticles using physical packaging. The method is simple to operate and has good universality. However, there are also defects, for example, the luminescent material leaks easily from the nanoparticles, the particle size of the nanomaterials prepared in different batches is not uniform, and the encapsulation rate of the materials is different. Therefore, searching for efficient functionalization methods for luminescent materials is still one of the core issues in the design and development of new luminescent materials.

In the decades since the development of polymeric nanomaterials in the field of optics, researchers have conducted a lot of work on synthesis control and material selection. While making breakthroughs, there is still demand for both high-performance and multifunctional materials. This also poses a higher challenge to the application of fluorescent polymer nanomaterials and biological fields. This is mainly reflected in the following aspects:

- (a) Fluorescent materials should be combined with current scientific theories and technologies. With advancements in science and technology, optical materials, as a traditional research field, can be further developed in the direction of diversification, high technology, and high performance when combined with advanced theory and technology. Thus, new subject areas are created [154,155].
- (b) Quantification of the structure–property relationship of multifunctional fluorescent polymer nanomaterials: Just as researchers have studied the “wetting” and “dewetting” of polymer-grafted core–shell particles in the matrix [156,157], essentially, the quantification of the effect of this structure on light transparency has developed from simple conclusions to a formalized theory. This method can be continued and expanded upon for other properties, forming quantitative structure–effect relationships for various properties.

- (c) The trade-off between key properties in the design of optical materials: The discussion in this article maintains a relatively consistent train of thought with most of the work. That is, starting from the material with a certain performance, the study on the impact of the structure on the improvement of this single performance, while ignoring the impact on other performances, or even the actual application environment. This is not conducive to the multifunctionalization of optical materials. Starting from key structural factors such as particle size, grafting, and loading in the structure of hybrid materials, the synergistic effects of a certain change in structure on various properties can be discussed to form an application-oriented material performance trade-off strategy.
- (d) Attention paid to the development of new optical functional materials: In addition to paying attention to the development of new photofunctional inorganic materials or polymer materials, we also need to pay attention to the development of new hybrid material systems. Carbonized polymer dots (CPDs) are a new type of nanofunctional elementary material that represent a new system of polymer nanohybridization [158,159]. In recent years, the advantages of this material have been reflected in its luminescent properties, and its synthesis process is considered to be a crosslinking carbonization process involving small molecules or polymer precursors. After several years of exploration, a family of CPDs with various luminescent properties such as full-color luminescence and narrow half-peak width emission has been obtained. Recently, Yang et al. further designed and applied this material to a material with both light transmission and mechanical properties, realizing the application of CPDs in the field of transparent optical films [160]. In addition, CPDs have also demonstrated their contributions in multiple fields such as imaging, sensing, and energy [161]. Their advantages such as low toxicity, environmental friendliness, and structural designability [162] lead us to believe that the introduction of new material systems such as CPDs will provide more excellent performance and broader application prospects for multifunctional fluorescent polymer nanomaterials.
- (e) In order to promote the further application of fluorescent polymer nanomaterials in biomedicine, future research work can be optimized and expanded in the following aspects. At present, most light-emitting polymers have low light-emitting performance in NIR-II. The development of NIR-II light-emitting polymer materials with higher luminous intensity or photothermal efficiency using DA structure adjustment combined with theoretical calculations is still one of the important research directions for the future. Efficient enrichment of luminescent nanofunctional materials in tumor sites is another key to improving the efficiency of tumor diagnosis and treatment. Using rational molecular design, targeting groups can be effectively bonded to polymer chains to prepare light-emitting polymers with targeting functions, which is of great significance for the precise diagnosis and treatment of tumor sites. A single treatment for tumors is gradually being replaced by multimodal treatment. The therapeutic effect on tumors can be improved by constructing a multifunctional nanodiagnosis and treatment platform with properties such as chemotherapy, photodynamic therapy, or photothermal therapy.
- (f) Internal/external stimuli-responsive fluorescent polymer nanoparticles that can be used in theranostics and sensing applications cannot be ignored either [163]. In particular, they respond to internal stimuli, including redox, pH, and enzymes, and external stimuli, including temperature, light, and magnetic fields, for drug delivery and sensing applications [164,165]. In terms of generating stimulus-responsive signals, these signals allow for amplification and easy detection of biologically relevant events. More detailed modeling of the photophysical properties of existing materials and their properties will provide decisive input for designing better performing NPs.

Author Contributions: Conceptualization, D.S. and K.S.; investigation, D.H. and Q.B.; writing—original draft preparation, P.L., W.L. and Y.X. All authors have read and agreed to the published version of the manuscript.

Funding: This work was supported by the Jilin Provincial Department of Education Science and Technology Research Planning Project (JJKH20220833KJ), Natural Science Foundation Project of Jilin Provincial Department of Science and Technology (YDZJ202301ZYTS348, YDZJ202101ZYTS092), Natural Science Foundation Projects of CCNU (CSJJ2022002ZK).

Institutional Review Board Statement: Not applicable.

Informed Consent Statement: Not applicable.

Data Availability Statement: Not applicable.

Conflicts of Interest: The authors declare no conflict of interest.

References

1. Yu, F.; Han, X.; Chen, L. Fluorescent probes for hydrogen sulfide detection and bioimaging. *Chem. Commun.* **2014**, *50*, 12234–12249. [[CrossRef](#)]
2. Guo, Z.; Park, S.; Yoon, J.; Shin, I. Recent progress in the development of near-infrared fluorescent probes for bioimaging applications. *Chem. Soc. Rev.* **2014**, *43*, 16–29. [[CrossRef](#)]
3. Abelha, T.F.; Dreiss, C.A.; Green, M.A.; Dailey, L.A. Conjugated polymers as nanoparticle probes for fluorescence and photoacoustic imaging. *J. Mater. Chem. B* **2020**, *8*, 592–606. [[CrossRef](#)] [[PubMed](#)]
4. Kim, S.-B.; Paulmurugan, R. Bioluminescent imaging systems for assay developments. *Anal. Sci.* **2021**, *37*, 233–247. [[CrossRef](#)]
5. Kim, S.-B.; Furuta, T.; Ohmuro-Matsuyama, Y.; Kitada, N.; Nishihara, R.; Maki, S.A. Bioluminescent imaging systems boosting near-infrared signals in mammalian cells. *Photochem. Photobiol. Sci.* **2023**, *2023*, 1–12. [[CrossRef](#)] [[PubMed](#)]
6. Yamada, K.; Nishizono, A. In Vivo Bioluminescent Imaging of Rabies Virus Infection and Evaluation of Antiviral Drug. In *Bioluminescence: Methods and Protocols*; Springer: Berlin/Heidelberg, Germany, 2022; Volume 1, pp. 347–352.
7. Sivaraman, G.; Iniya, M.; Anand, T.; Kotla, N.G.; Sunnapu, O.; Singaravadevel, S.; Gulyani, A.; Chellappa, D. Chemically diverse small molecule fluorescent chemosensors for copper ion. *Coord. Chem. Rev.* **2018**, *357*, 50–104. [[CrossRef](#)]
8. Yang, J.; Yang, Y.W. Metal–organic frameworks for biomedical applications. *Small* **2020**, *16*, 1906846. [[CrossRef](#)]
9. Liu, X.; Sun, X.; Liang, G. Peptide-based supramolecular hydrogels for bioimaging applications. *Biomater. Sci.* **2021**, *9*, 315–327. [[CrossRef](#)]
10. Michalet, X.; Pinaud, F.F.; Bentolila, L.A.; Tsay, J.M.; Doose, S.; Li, J.J.; Sundaresan, G.; Wu, A.; Gambhir, S.; Weiss, S. Quantum dots for live cells, in vivo imaging, and diagnostics. *Science* **2005**, *307*, 538–544. [[CrossRef](#)]
11. Shen, M.; Kong, F.; Tong, L.; Luo, Y.; Yin, S.; Liu, C.; Zhang, P.; Wang, L.; Chu, P.K.; Ding, Y. Carbon capture and storage (CCS): Development path based on carbon neutrality and economic policy. *Carbon Neutrality* **2022**, *1*, 37. [[CrossRef](#)]
12. Wang, F.; Tan, W.B.; Zhang, Y.; Fan, X.; Wang, M. Luminescent nanomaterials for biological labelling. *Nanotechnology* **2005**, *17*, R1. [[CrossRef](#)]
13. Mako, T.L.; Racicot, J.M.; Levine, M. Supramolecular luminescent sensors. *Chem. Rev.* **2018**, *119*, 322–477. [[CrossRef](#)]
14. Shen, M.; Ma, H. Metal-organic frameworks (MOFs) and their derivative as electrode materials for lithium-ion batteries. *Coord. Chem. Rev.* **2022**, *470*, 214715. [[CrossRef](#)]
15. Wang, Y.; Feng, L.; Wang, S. Conjugated polymer nanoparticles for imaging, cell activity regulation, and therapy. *Adv. Funct. Mater.* **2019**, *29*, 1806818. [[CrossRef](#)]
16. Zhu, S.; Tian, R.; Antaris, A.L.; Chen, X.; Dai, H. Near-infrared-II molecular dyes for cancer imaging and surgery. *Adv. Mater.* **2019**, *31*, 1900321. [[CrossRef](#)]
17. Li, T.; Liu, J.; Sun, X.-L.; Wan, W.-M.; Xiao, L.; Qian, Q. Boronic acid-containing polymeric nanomaterials via polymerization induced self-assembly as fructose sensor. *Polymer* **2022**, *253*, 125005. [[CrossRef](#)]
18. Abraham, J.E.; Balachandran, M. Fluorescent Mechanism in Zero-Dimensional Carbon Nanomaterials: A Review. *J. Fluoresc.* **2022**, *32*, 887–906. [[CrossRef](#)] [[PubMed](#)]
19. Zhai, S.; Chen, H.; Zhang, Y.; Li, P.; Wu, W. Nanocellulose: A promising nanomaterial for fabricating fluorescent composites. *Cellulose* **2022**, *29*, 7011–7035. [[CrossRef](#)]
20. Shen, M.; Tong, L.; Yin, S.; Liu, C.; Wang, L.; Feng, W.; Ding, Y. Cryogenic technology progress for CO₂ capture under carbon neutrality goals: A review. *Sep. Purif. Technol.* **2022**, *2022*, 121734. [[CrossRef](#)]
21. Manivasagan, P.; Kim, J.; Jang, E.-S. Recent progress in multifunctional conjugated polymer nanomaterial-based synergistic combination phototherapy for microbial infection theranostics. *Coord. Chem. Rev.* **2022**, *470*, 214701. [[CrossRef](#)]
22. Chauhan, N.; Saxena, K.; Jain, U. Smart nanomaterials employed recently for drug delivery in cancer therapy: An intelligent approach. *BioNanoScience* **2022**, *12*, 1356–1365. [[CrossRef](#)]
23. Shen, X.; Xu, W.; Ouyang, J.; Na, N. Fluorescence resonance energy transfer-based nanomaterials for the sensing in biological systems. *Chin. Chem. Lett.* **2022**, *33*, 4505–4516. [[CrossRef](#)]

24. Yang, X.; Qin, X.; Ji, H.; Du, L.; Li, M. Constructing firefly luciferin bioluminescence probes for in vivo imaging. *Org. Biomol. Chem.* **2022**, *20*, 1360–1372. [[CrossRef](#)] [[PubMed](#)]
25. Afshari, M.J.; Li, C.; Zeng, J.; Cui, J.; Wu, S.; Gao, M. Self-illuminating NIR-II bioluminescence imaging probe based on silver sulfide quantum dots. *ACS Nano* **2022**, *16*, 16824–16832. [[CrossRef](#)] [[PubMed](#)]
26. Yoon, S.; Cheon, S.Y.; Park, S.; Lee, D.; Lee, Y.; Han, S.; Kim, M.; Koo, H. Recent advances in optical imaging through deep tissue: Imaging probes and techniques. *Biomater. Res.* **2022**, *26*, 57. [[CrossRef](#)]
27. Elsbahy, M.; Heo, G.S.; Lim, S.-M.; Sun, G.; Wooley, K.L. Polymeric nanostructures for imaging and therapy. *Chem. Rev.* **2015**, *115*, 10967–11011. [[CrossRef](#)]
28. Smith, B.R.; Gambhir, S.S. Nanomaterials for in vivo imaging. *Chem. Rev.* **2017**, *117*, 901–986. [[CrossRef](#)] [[PubMed](#)]
29. Wang, B.; Zhou, X.-Q.; Li, L.; Li, Y.-X.; Yu, L.-P.; Chen, Y. Ratiometric fluorescence sensor for point-of-care testing of bilirubin based on tetraphenylethylene functionalized polymer nanoaggregate and rhodamine B. *Sens. Actuators B Chem.* **2022**, *369*, 132392. [[CrossRef](#)]
30. Ahumada, G.; Borkowska, M. Fluorescent polymers conspectus. *Polymers* **2022**, *14*, 1118. [[CrossRef](#)]
31. Bou, S.; Klymchenko, A.S.; Collot, M. Fluorescent labeling of biocompatible block copolymers: Synthetic strategies and applications in bioimaging. *Mater. Adv.* **2021**, *2*, 3213–3233. [[CrossRef](#)]
32. Zhang, P.; Xue, M.; Lin, Z.; Yang, H.; Zhang, C.; Cui, J.; Chen, J. Aptamer functionalization and high-contrast reversible dual-color photoswitching fluorescence of polymeric nanoparticles for latent fingerprints imaging. *Sens. Actuators B Chem.* **2022**, *367*, 132049. [[CrossRef](#)]
33. Mohammadi, R.; Naderi-Manesh, H.; Farzin, L.; Vaezi, Z.; Ayarri, N.; Samandari, L.; Shamsipur, M. Fluorescence sensing and imaging with carbon-based quantum dots for early diagnosis of cancer: A review. *J. Pharm. Biomed. Anal.* **2022**, *212*, 114628. [[CrossRef](#)]
34. Wan, W.; Li, Z.; Wang, X.; Tian, F.; Yang, J. Surface-fabrication of fluorescent hydroxyapatite for cancer cell imaging and bio-printing applications. *Biosensors* **2022**, *12*, 419. [[CrossRef](#)]
35. Jiang, M.-C.; Liu, H.-B.; Wang, J.-Q.; Li, S.; Zheng, Z.; Wang, D.; Wei, H.; Yu, C.-Y. Optimized aptamer functionalization for enhanced anticancer efficiency in vivo. *Int. J. Pharm.* **2022**, *628*, 122330. [[CrossRef](#)] [[PubMed](#)]
36. Nerantzaki, M.; Michel, A.; Petit, L.; Garnier, M.; Ménager, C.; Griffete, N. Biotinylated magnetic molecularly imprinted polymer nanoparticles for cancer cell targeting and controlled drug delivery. *Chem. Commun.* **2022**, *58*, 5642–5645. [[CrossRef](#)] [[PubMed](#)]
37. Shou, K.; Tang, Y.; Chen, H.; Chen, S.; Zhang, L.; Zhang, A.; Fan, Q.; Yu, A.; Cheng, Z. Diketopyrrolopyrrole-based semiconducting polymer nanoparticles for in vivo second near-infrared window imaging and image-guided tumor surgery. *Chem. Sci.* **2018**, *9*, 3105–3110. [[CrossRef](#)]
38. Zhang, Q.; Wang, X.; Cong, Y.; Kang, Y.; Wu, Z.; Li, L. Conjugated polymer-functionalized stretchable supramolecular hydrogels to monitor and control cellular behavior. *ACS Appl. Mater. Interfaces* **2022**, *14*, 12674–12683. [[CrossRef](#)]
39. Hamadani, C.M.; Chandrasiri, I.; Yaddehige, M.L.; Dasanayake, G.S.; Owolabi, I.; Flynt, A.; Hossain, M.; Liberman, L.; Lodge, T.P.; Werfel, T.A. Improved nanoformulation and bio-functionalization of linear-dendritic block copolymers with biocompatible ionic liquids. *Nanoscale* **2022**, *14*, 6021–6036. [[CrossRef](#)] [[PubMed](#)]
40. Sun, H.; Schanze, K.S. Functionalization of water-soluble conjugated polymers for bioapplications. *ACS Appl. Mater. Interfaces* **2022**, *14*, 20506–20519. [[CrossRef](#)]
41. Nothling, M.D.; Bailey, C.G.; Fillbrook, L.L.; Wang, G.; Gao, Y.; McCamey, D.R.; Monfared, M.; Wong, S.; Beves, J.E.; Stenzel, M.H. Polymer grafting to polydopamine free radicals for universal surface functionalization. *J. Am. Chem. Soc.* **2022**, *144*, 6992–7000. [[CrossRef](#)]
42. Chatterjee, S.; Lou, X.-Y.; Liang, F.; Yang, Y.-W. Surface-functionalized gold and silver nanoparticles for colorimetric and fluorescent sensing of metal ions and biomolecules. *Coord. Chem. Rev.* **2022**, *459*, 214461. [[CrossRef](#)]
43. Shahi, S.; Roghani-Mamaqani, H.; Talebi, S.; Mardani, H. Stimuli-responsive destructible polymeric hydrogels based on irreversible covalent bond dissociation. *Polym. Chem.* **2022**, *13*, 161–192. [[CrossRef](#)]
44. Nifant'ev, I.; Besprozvannykh, V.; Shlyakhtin, A.; Tavtorkin, A.; Legkov, S.; Chinova, M.; Arutyunyan, I.; Soboleva, A.; Fatkhudinov, T.; Ivchenko, P. Chain-End Functionalization of Poly (ϵ -caprolactone) for Chemical Binding with Gelatin: Binary Electrospun Scaffolds with Improved Physico-Mechanical Characteristics and Cell Adhesive Properties. *Polymers* **2022**, *14*, 4203. [[CrossRef](#)]
45. Lorandi, F.; Fantin, M.; Matyjaszewski, K. Atom Transfer Radical Polymerization: A Mechanistic Perspective. *J. Am. Chem. Soc.* **2022**, *144*, 15413–15430. [[CrossRef](#)] [[PubMed](#)]
46. Dworakowska, S.; Lorandi, F.; Gorczyński, A.; Matyjaszewski, K. Toward green atom transfer radical polymerization: Current status and future challenges. *Adv. Sci.* **2022**, *9*, 2106076. [[CrossRef](#)]
47. Kim, J.; Cattoz, B.; Leung, A.H.; Parish, J.D.; Becer, C.R. Enabling Reversible Addition-Fragmentation Chain-Transfer Polymerization for Brush Copolymers with a Poly (2-oxazoline) Backbone. *Macromolecules* **2022**, *55*, 4411–4419. [[CrossRef](#)]
48. Wang, J.-S.; Matyjaszewski, K. Controlled/"living" radical polymerization. atom transfer radical polymerization in the presence of transition-metal complexes. *J. Am. Chem. Soc.* **1995**, *117*, 5614–5615. [[CrossRef](#)]
49. Kato, M.; Kamigaito, M.; Sawamoto, M.; Higashimura, T. Polymerization of methyl methacrylate with the carbon tetrachloride/dichlorotris-(triphenylphosphine) ruthenium (II)/methylaluminum bis (2, 6-di-tert-butylphenoxide) initiating system: Possibility of living radical polymerization. *Macromolecules* **1995**, *28*, 1721–1723. [[CrossRef](#)]
50. Matyjaszewski, K.; Xia, J. Atom transfer radical polymerization. *Chem. Rev.* **2001**, *101*, 2921–2990. [[CrossRef](#)]

51. Coessens, V.; Pintauer, T.; Matyjaszewski, K. Functional polymers by atom transfer radical polymerization. *Prog. Polym. Sci.* **2001**, *26*, 337–377. [[CrossRef](#)]
52. Pan, X.; Fantin, M.; Yuan, F.; Matyjaszewski, K. Externally controlled atom transfer radical polymerization. *Chem. Soc. Rev.* **2018**, *47*, 5457–5490. [[CrossRef](#)] [[PubMed](#)]
53. Yuan, M.; Cui, X.; Zhu, W.; Tang, H. Development of environmentally friendly atom transfer radical polymerization. *Polymers* **2020**, *12*, 1987. [[CrossRef](#)] [[PubMed](#)]
54. Chakma, P.; Zeitler, S.M.; Baum, F.; Yu, J.; Shindy, W.; Pozzo, L.D.; Golder, M.R. Mechanoredox Catalysis Enables a Sustainable and Versatile Reversible Addition-Fragmentation Chain Transfer Polymerization Process. *Angew. Chem. Int. Ed.* **2023**, *62*, e202215733. [[CrossRef](#)] [[PubMed](#)]
55. Bradford, K.G.; Petit, L.M.; Whitfield, R.; Anastasaki, A.; Barner-Kowollik, C.; Konkolewicz, D. Ubiquitous Nature of Rate Retardation in Reversible Addition-Fragmentation Chain Transfer Polymerization. *J. Am. Chem. Soc.* **2021**, *143*, 17769–17777. [[CrossRef](#)]
56. Chiefari, J.; Chong, Y.; Ercole, F.; Krstina, J.; Jeffery, J.; Le, T.P.; Mayadunne, R.T.; Meijs, G.F.; Moad, C.L.; Moad, G. Living free-radical polymerization by reversible addition-fragmentation chain transfer: The RAFT process. *Macromolecules* **1998**, *31*, 5559. [[CrossRef](#)]
57. Moad, G.; Chiefari, J.; Chong, Y.K.; Krstina, J.; Mayadunne, R.T.A.; Postma, A.; Rizzardo, E.; Thang, S.H. Living free radical polymerization with reversible addition-fragmentation chain transfer (the life of RAFT). *Polym. Int.* **2000**, *49*, 993–1001. [[CrossRef](#)]
58. Li, M.; Fromel, M.; Ranaweera, D.; Rocha, S.; Boyer, C.; Pester, C.W. SI-PET-RAFT: Surface-initiated photoinduced electron transfer-reversible addition-fragmentation chain transfer polymerization. *ACS Macro Lett.* **2019**, *8*, 374–380. [[CrossRef](#)]
59. Zhang, X.; Yang, Z.; Jiang, Y.; Liao, S. Organocatalytic, stereoselective, cationic reversible addition-fragmentation chain-transfer polymerization of vinyl ethers. *J. Am. Chem. Soc.* **2021**, *144*, 679–684. [[CrossRef](#)]
60. Cheng, G.; Xu, D.; Lu, Z.; Liu, K. Chiral self-assembly of nanoparticles induced by polymers synthesized via reversible addition-fragmentation chain transfer polymerization. *ACS Nano* **2019**, *13*, 1479–1489. [[CrossRef](#)]
61. Strover, L.T.; Postma, A.; Horne, M.D.; Moad, G. Anthraquinone-mediated reduction of a trithiocarbonate chain-transfer agent to initiate electrochemical reversible addition-fragmentation chain transfer polymerization. *Macromolecules* **2020**, *53*, 10315–10322. [[CrossRef](#)]
62. Tuncel, D.; Demir, H.V. Conjugated polymer nanoparticles. *Nanoscale* **2010**, *2*, 484–494. [[CrossRef](#)]
63. Feng, L.; Zhu, C.; Yuan, H.; Liu, L.; Lv, F.; Wang, S. Conjugated polymer nanoparticles: Preparation, properties, functionalization and biological applications. *Chem. Soc. Rev.* **2013**, *42*, 6620–6633. [[CrossRef](#)]
64. Kurokawa, N.; Yoshikawa, H.; Hirota, N.; Hyodo, K.; Masuhara, H. Size-dependent spectroscopic properties and thermochromic behavior in poly (substituted thiophene) nanoparticles. *ChemPhysChem* **2004**, *5*, 1609–1615. [[CrossRef](#)]
65. Wu, C.; Szymanski, C.; McNeill, J. Preparation and encapsulation of highly fluorescent conjugated polymer nanoparticles. *Langmuir* **2006**, *22*, 2956–2960. [[CrossRef](#)] [[PubMed](#)]
66. Wu, C.; Hansen, S.J.; Hou, Q.; Yu, J.; Zeigler, M.; Jin, Y.; Burnham, D.R.; McNeill, J.D.; Olson, J.M.; Chiu, D.T. Design of highly emissive polymer dot bioconjugates for in vivo tumor targeting. *Angew. Chem.* **2011**, *123*, 3492–3496. [[CrossRef](#)]
67. Rivas, C.J.M.; Tarhini, M.; Badri, W.; Miladi, K.; Greige-Gerges, H.; Nazari, Q.A.; Rodríguez, S.A.G.; Román, R.Á.; Fessi, H.; Elaissari, A. Nanoprecipitation process: From encapsulation to drug delivery. *Int. J. Pharm.* **2017**, *532*, 66–81. [[CrossRef](#)]
68. Vodyashkin, A.A.; Kezimana, P.; Vetcher, A.A.; Stanishkevskiy, Y.M. Biopolymeric nanoparticles–multifunctional materials of the future. *Polymers* **2022**, *14*, 2287. [[CrossRef](#)]
69. Kang, S.; Yoon, T.W.; Kim, G.-Y.; Kang, B. Review of Conjugated Polymer Nanoparticles: From Formulation to Applications. *ACS Appl. Nano Mater.* **2022**, *5*, 17436–17460. [[CrossRef](#)]
70. Wang, Q.-B.; Zhang, C.-J.; Yu, H.; Zhang, X.; Lu, Q.; Yao, J.-S.; Zhao, H. The sensitive “Turn-on” fluorescence platform of ascorbic acid based on conjugated polymer nanoparticles. *Anal. Chim. Acta* **2020**, *1097*, 153–160. [[CrossRef](#)]
71. Fang, F.; Li, M.; Zhang, J.; Lee, C.-S. Different strategies for organic nanoparticle preparation in biomedicine. *ACS Mater. Lett.* **2020**, *2*, 531–549. [[CrossRef](#)]
72. MacFarlane, L.R.; Shaikh, H.; Garcia-Hernandez, J.D.; Vespa, M.; Fukui, T.; Manners, I. Functional nanoparticles through π -conjugated polymer self-assembly. *Nat. Rev. Mater.* **2021**, *6*, 7–26. [[CrossRef](#)]
73. Ong, S.Y.; Zhang, C.; Dong, X.; Yao, S.Q. Recent advances in polymeric nanoparticles for enhanced fluorescence and photoacoustic imaging. *Angew. Chem. Int. Ed.* **2021**, *60*, 17797–17809. [[CrossRef](#)]
74. Sur, S.; Rathore, A.; Dave, V.; Reddy, K.R.; Chouhan, R.S.; Sadhu, V. Recent developments in functionalized polymer nanoparticles for efficient drug delivery system. *Nano-Struct. Nano Objects* **2019**, *20*, 100397. [[CrossRef](#)]
75. Indoria, S.; Singh, V.; Hsieh, M.-F. Recent advances in theranostic polymeric nanoparticles for cancer treatment: A review. *Int. J. Pharm.* **2020**, *582*, 119314. [[CrossRef](#)] [[PubMed](#)]
76. Cölfen, H. Double-hydrophilic block copolymers: Synthesis and application as novel surfactants and crystal growth modifiers. *Macromol. Rapid Commun.* **2001**, *22*, 219–252. [[CrossRef](#)]
77. Gaucher, G.; Dufresne, M.-H.; Sant, V.P.; Kang, N.; Maysinger, D.; Leroux, J.-C. Block copolymer micelles: Preparation, characterization and application in drug delivery. *J. Control. Release* **2005**, *109*, 169–188. [[CrossRef](#)] [[PubMed](#)]
78. Chen, J.Z.; Zhao, Q.L.; Lu, H.C.; Huang, J.; Cao, S.K.; Ma, Z. Polymethylene-b-polystyrene diblock copolymer: Synthesis, property, and application. *J. Polym. Sci. Part A Polym. Chem.* **2010**, *48*, 1894–1900. [[CrossRef](#)]

79. Zhou, Y.; Wang, Z.; Wang, Y.; Li, L.; Zhou, N.; Cai, Y.; Zhang, Z.; Zhu, X. Azoreductase-triggered fluorescent nanoprobe synthesized by RAFT-mediated polymerization-induced self-assembly for drug release. *Polym. Chem.* **2020**, *11*, 5619–5629. [[CrossRef](#)]
80. Sun, H.; Cao, W.; Zang, N.; Clemons, T.D.; Scheutz, G.M.; Hu, Z.; Thompson, M.P.; Liang, Y.; Vratsanos, M.; Zhou, X. Proapoptotic Peptide Brush Polymer Nanoparticles via Photoinitiated Polymerization-Induced Self-Assembly. *Angew. Chem.* **2020**, *132*, 19298–19304. [[CrossRef](#)]
81. Khor, S.Y.; Quinn, J.F.; Whittaker, M.R.; Truong, N.P.; Davis, T.P. Controlling nanomaterial size and shape for biomedical applications via polymerization-induced self-assembly. *Macromol. Rapid Commun.* **2019**, *40*, 1800438. [[CrossRef](#)]
82. Ramkumar, R.; Sundaram, M.M. A biopolymer gel-decorated cobalt molybdate nanowafer: Effective graft polymer cross-linked with an organic acid for better energy storage. *New J. Chem.* **2016**, *40*, 2863–2877. [[CrossRef](#)]
83. Ferguson, C.J.; Hughes, R.J.; Nguyen, D.; Pham, B.T.; Gilbert, R.G.; Serelis, A.K.; Such, C.H.; Hawket, B.S. Ab initio emulsion polymerization by RAFT-controlled self-assembly. *Macromolecules* **2005**, *38*, 2191–2204. [[CrossRef](#)]
84. Wan, W.-M.; Hong, C.-Y.; Pan, C.-Y. One-pot synthesis of nanomaterials via RAFT polymerization induced self-assembly and morphology transition. *Chem. Commun.* **2009**, *39*, 5883–5885. [[CrossRef](#)] [[PubMed](#)]
85. Wan, W.-M.; Sun, X.-L.; Pan, C.-Y. Morphology transition in RAFT polymerization for formation of vesicular morphologies in one pot. *Macromolecules* **2009**, *42*, 4950–4952. [[CrossRef](#)]
86. Canning, S.L.; Smith, G.N.; Armes, S.P. A critical appraisal of RAFT-mediated polymerization-induced self-assembly. *Macromolecules* **2016**, *49*, 1985–2001. [[CrossRef](#)] [[PubMed](#)]
87. Buwalda, S.J.; Vermonden, T.; Hennink, W.E. Hydrogels for therapeutic delivery: Current developments and future directions. *Biomacromolecules* **2017**, *18*, 316–330. [[CrossRef](#)]
88. Zhang, M.; Huang, Y.; Pan, W.; Tong, X.; Zeng, Q.; Su, T.; Qi, X.; Shen, J. Polydopamine-incorporated dextran hydrogel drug carrier with tailorable structure for wound healing. *Carbohydr. Polym.* **2021**, *253*, 117213. [[CrossRef](#)]
89. Ilgin, P.; Ozay, H.; Ozay, O. Synthesis and characterization of pH responsive alginate based-hydrogels as oral drug delivery carrier. *J. Polym. Res.* **2020**, *27*, 251. [[CrossRef](#)]
90. Kabanov, A.V.; Vinogradov, S.V. Nanogels as pharmaceutical carriers: Finite networks of infinite capabilities. *Angew. Chem. Int. Ed.* **2009**, *48*, 5418–5429. [[CrossRef](#)]
91. Oh, J.K.; Drumright, R.; Siegwart, D.J.; Matyjaszewski, K. The development of microgels/nanogels for drug delivery applications. *Prog. Polym. Sci.* **2008**, *33*, 448–477. [[CrossRef](#)]
92. Nishizawa, Y.; Minato, H.; Inui, T.; Uchihashi, T.; Suzuki, D. Nanostructures, thermoresponsiveness, and assembly mechanism of hydrogel microspheres during aqueous free-radical precipitation polymerization. *Langmuir* **2020**, *37*, 151–159. [[CrossRef](#)] [[PubMed](#)]
93. Bai, F.; Yang, X.; Huang, W. Synthesis of narrow or monodisperse poly (divinylbenzene) microspheres by distillation– precipitation polymerization. *Macromolecules* **2004**, *37*, 9746–9752. [[CrossRef](#)]
94. Fan, M.; Wang, F.; Wang, C. Reflux precipitation polymerization: A new platform for the preparation of uniform polymeric nanogels for biomedical applications. *Macromol. Biosci.* **2018**, *18*, 1800077. [[CrossRef](#)]
95. Aillon, K.L.; Xie, Y.; El-Gendy, N.; Berkland, C.J.; Forrest, M.L. Effects of nanomaterial physicochemical properties on in vivo toxicity. *Adv. Drug Deliv. Rev.* **2009**, *61*, 457–466. [[CrossRef](#)]
96. Rama Narsimha Reddy, A.; Narsimha Reddy, Y.; Himabindu, V.; Rama Krishna, D. Induction of oxidative stress and cytotoxicity by carbon nanomaterials is dependent on physical properties. *Toxicol. Ind. Health* **2011**, *27*, 3–10. [[CrossRef](#)] [[PubMed](#)]
97. Mahmoudi, M.; Shokrgozar, M.A.; Sardari, S.; Moghadam, M.K.; Vali, H.; Laurent, S.; Stroeve, P. Irreversible changes in protein conformation due to interaction with superparamagnetic iron oxide nanoparticles. *Nanoscale* **2011**, *3*, 1127–1138. [[CrossRef](#)]
98. Liu, J.-Y.; Zhao, L.-Y.; Wang, Y.-Y.; Li, D.-Y.; Tao, D.; Li, L.-Y.; Tang, J.-T. Magnetic stent hyperthermia for esophageal cancer: An in vitro investigation in the ECA-109 cell line. *Oncol. Rep.* **2012**, *27*, 791–797.
99. Lanone, S.; Boczkowski, J. Biomedical applications and potential health risks of nanomaterials: Molecular mechanisms. *Curr. Mol. Med.* **2006**, *6*, 651–663. [[CrossRef](#)]
100. Rahman, I. Regulation of nuclear factor- κ B, activator protein-1, and glutathione levels by tumor necrosis factor- α and dexamethasone in alveolar epithelial cells. *Biochem. Pharmacol.* **2000**, *60*, 1041–1049. [[CrossRef](#)]
101. Rahman, I.; Biswas, S.K.; Jimenez, L.A.; Torres, M.; Forman, H.J. Glutathione, stress responses, and redox signaling in lung inflammation. *Antioxid. Redox Signal.* **2005**, *7*, 42–59. [[CrossRef](#)]
102. Guanming, Q.; Xikum, L.; Tai, Q.; Haitao, Z.; Honghao, Y.; Ruiting, M. Application of rare earths in advanced ceramic materials. *J. Rare Earths* **2007**, *25*, 281–286. [[CrossRef](#)]
103. Heffern, M.C.; Matosziuk, L.M.; Meade, T.J. Lanthanide probes for bioresponsive imaging. *Chem. Rev.* **2014**, *114*, 4496–4539. [[CrossRef](#)]
104. Zhang, C.; Zhang, C.; Zhang, Z.; He, T.; Mi, X.; Kong, T.; Fu, Z.; Zheng, H.; Xu, H. Self-suspended rare-earth doped up-conversion luminescent waveguide: Propagating and directional radiation. *Opto-Electron. Adv.* **2020**, *3*, 190045. [[CrossRef](#)]
105. Zhu, X.; Zhang, J.; Liu, J.; Zhang, Y. Recent progress of rare-earth doped upconversion nanoparticles: Synthesis, optimization, and applications. *Adv. Sci.* **2019**, *6*, 1901358. [[CrossRef](#)]
106. Werts, M.H. Making sense of lanthanide luminescence. *Sci. Prog.* **2005**, *88*, 101–131. [[CrossRef](#)]

107. Montgomery, C.P.; Murray, B.S.; New, E.J.; Pal, R.; Parker, D. Cell-penetrating metal complex optical probes: Targeted and responsive systems based on lanthanide luminescence. *Acc. Chem. Res.* **2009**, *42*, 925–937. [[CrossRef](#)] [[PubMed](#)]
108. Moore, E.G.; Samuel, A.P.; Raymond, K.N. From antenna to assay: Lessons learned in lanthanide luminescence. *Acc. Chem. Res.* **2009**, *42*, 542–552. [[CrossRef](#)]
109. Ding, Z.; He, Y.; Rao, H.; Zhang, L.; Nguyen, W.; Wang, J.; Wu, Y.; Han, C.; Xing, C.; Yan, C. Novel Fluorescent Probe Based on Rare-Earth Doped Upconversion Nanomaterials and Its Applications in Early Cancer Detection. *Nanomaterials* **2022**, *12*, 1787. [[CrossRef](#)] [[PubMed](#)]
110. Li, H.; Wei, R.; Yan, G.-H.; Sun, J.; Li, C.; Wang, H.; Shi, L.; Capobianco, J.A.; Sun, L. Smart self-assembled nanosystem based on water-soluble pillararene and rare-earth-doped upconversion nanoparticles for ph-responsive drug delivery. *ACS Appl. Mater. Interfaces* **2018**, *10*, 4910–4920. [[CrossRef](#)]
111. Sun, L.-D.; Wang, Y.-F.; Yan, C.-H. Paradigms and challenges for bioapplication of rare earth upconversion luminescent nanoparticles: Small size and tunable emission/excitation spectra. *Acc. Chem. Res.* **2014**, *47*, 1001–1009. [[CrossRef](#)]
112. Cardoso Dos Santos, M.; Runser, A.; Bartenlian, H.; Nonat, A.M.; Charbonnière, L.J.; Klymchenko, A.S.; Hildebrandt, N.; Reisch, A. Lanthanide-complex-loaded polymer nanoparticles for background-free single-particle and live-cell imaging. *Chem. Mater.* **2019**, *31*, 4034–4041. [[CrossRef](#)]
113. Ai, K.; Zhang, B.; Lu, L. Europium-based fluorescence nanoparticle sensor for rapid and ultrasensitive detection of an anthrax biomarker. *Angew. Chem.* **2009**, *121*, 310–314. [[CrossRef](#)]
114. Tan, H.; Liu, B.; Chen, Y. Lanthanide coordination polymer nanoparticles for sensing of mercury (II) by photoinduced electron transfer. *ACS Nano* **2012**, *6*, 10505–10511. [[CrossRef](#)]
115. Binnemans, K. Lanthanide-based luminescent hybrid materials. *Chem. Rev.* **2009**, *109*, 4283–4374. [[CrossRef](#)] [[PubMed](#)]
116. Xu, D.; Zhou, X.; Huang, Q.; Tian, J.; Huang, H.; Wan, Q.; Dai, Y.; Wen, Y.; Zhang, X.; Wei, Y. Facile fabrication of biodegradable lanthanide ions containing fluorescent polymeric nanoparticles: Characterization, optical properties and biological imaging. *Mater. Chem. Phys.* **2018**, *207*, 226–232. [[CrossRef](#)]
117. Xu, D.; Liu, M.; Huang, Q.; Chen, J.; Huang, H.; Deng, F.; Wen, Y.; Tian, J.; Zhang, X.; Wei, Y. One-step synthesis of europium complexes containing polyamino acids through ring-opening polymerization and their potential for biological imaging applications. *Talanta* **2018**, *188*, 1–6. [[CrossRef](#)]
118. Fan, Y.; Zhang, F. A new generation of NIR-II probes: Lanthanide-based nanocrystals for bioimaging and biosensing. *Adv. Opt. Mater.* **2019**, *7*, 1801417. [[CrossRef](#)]
119. Cai, Y.; Wei, Z.; Song, C.; Tang, C.; Han, W.; Dong, X. Optical nano-agents in the second near-infrared window for biomedical applications. *Chem. Soc. Rev.* **2019**, *48*, 22–37. [[CrossRef](#)]
120. Tao, Z.; Dang, X.; Huang, X.; Muzumdar, M.D.; Xu, E.S.; Bardhan, N.M.; Song, H.; Qi, R.; Yu, Y.; Li, T. Early tumor detection afforded by in vivo imaging of near-infrared II fluorescence. *Biomaterials* **2017**, *134*, 202–215. [[CrossRef](#)]
121. Dimov, I.B.; Moser, M.; Malliaras, G.G.; McCulloch, I. Semiconducting polymers for neural applications. *Chem. Rev.* **2022**, *122*, 4356–4396. [[CrossRef](#)]
122. Liu, C.; Wang, K.; Gong, X.; Heeger, A.J. Low bandgap semiconducting polymers for polymeric photovoltaics. *Chem. Soc. Rev.* **2016**, *45*, 4825–4846. [[CrossRef](#)]
123. Scharber, M.C.; Sariciftci, N.S. Low band gap conjugated semiconducting polymers. *Adv. Mater. Technol.* **2021**, *6*, 2000857. [[CrossRef](#)]
124. Yan, X.; Xiong, M.; Deng, X.-Y.; Liu, K.-K.; Li, J.-T.; Wang, X.-Q.; Zhang, S.; Prine, N.; Zhang, Z.; Huang, W. Approaching disorder-tolerant semiconducting polymers. *Nat. Commun.* **2021**, *12*, 5723. [[CrossRef](#)]
125. Tsai, W.K.; Chan, Y.H. Semiconducting polymer dots as near-infrared fluorescent probes for bioimaging and sensing. *J. Chin. Chem. Soc.* **2019**, *66*, 9–20. [[CrossRef](#)]
126. Xu, L.; Cheng, L.; Wang, C.; Peng, R.; Liu, Z. Conjugated polymers for photothermal therapy of cancer. *Polym. Chem.* **2014**, *5*, 1573–1580. [[CrossRef](#)]
127. Chen, P.; Ma, Y.; Zheng, Z.; Wu, C.; Wang, Y.; Liang, G. Facile syntheses of conjugated polymers for photothermal tumour therapy. *Nat. Commun.* **2019**, *10*, 1192. [[CrossRef](#)] [[PubMed](#)]
128. Li, S.; Wang, X.; Hu, R.; Chen, H.; Li, M.; Wang, J.; Wang, Y.; Liu, L.; Lv, F.; Liang, X.-J. Near-infrared (NIR)-absorbing conjugated polymer dots as highly effective photothermal materials for in vivo cancer therapy. *Chem. Mater.* **2016**, *28*, 8669–8675. [[CrossRef](#)]
129. Chen, J.; Wang, F.; Liu, Q.; Du, J. Antibacterial polymeric nanostructures for biomedical applications. *Chem. Commun.* **2014**, *50*, 14482–14493. [[CrossRef](#)] [[PubMed](#)]
130. Chong, H.; Nie, C.; Zhu, C.; Yang, Q.; Liu, L.; Lv, F.; Wang, S. Conjugated polymer nanoparticles for light-activated anticancer and antibacterial activity with imaging capability. *Langmuir* **2012**, *28*, 2091–2098. [[CrossRef](#)]
131. Li, J.; Zhao, Q.; Shi, F.; Liu, C.; Tang, Y. NIR-mediated nanohybrids of upconversion nanophosphors and fluorescent conjugated polymers for high-efficiency antibacterial performance based on fluorescence resonance energy transfer. *Adv. Healthc. Mater.* **2016**, *5*, 2967–2971. [[CrossRef](#)] [[PubMed](#)]
132. Zhang, K.; Tang, X.; Zhang, J.; Lu, W.; Lin, X.; Zhang, Y.; Tian, B.; Yang, H.; He, H. PEG–PLGA copolymers: Their structure and structure-influenced drug delivery applications. *J. Control. Release* **2014**, *183*, 77–86. [[CrossRef](#)] [[PubMed](#)]

133. Zhang, W.; Huang, T.; Li, J.; Sun, P.; Wang, Y.; Shi, W.; Han, W.; Wang, W.; Fan, Q.; Huang, W. Facial control intramolecular charge transfer of quinoid conjugated polymers for efficient in vivo NIR-II imaging. *ACS Appl. Mater. Interfaces* **2019**, *11*, 16311–16319. [[CrossRef](#)] [[PubMed](#)]
134. Hong, G.; Zou, Y.; Antaris, A.L.; Diao, S.; Wu, D.; Cheng, K.; Zhang, X.; Chen, C.; Liu, B.; He, Y. Ultrafast fluorescence imaging in vivo with conjugated polymer fluorophores in the second near-infrared window. *Nat. Commun.* **2014**, *5*, 4206. [[CrossRef](#)] [[PubMed](#)]
135. Qi, J.; Hu, X.; Dong, X.; Lu, Y.; Lu, H.; Zhao, W.; Wu, W. Towards more accurate bioimaging of drug nanocarriers: Turning aggregation-caused quenching into a useful tool. *Adv. Drug Deliv. Rev.* **2019**, *143*, 206–225. [[CrossRef](#)]
136. Wang, B.W.; Jiang, K.; Li, J.X.; Luo, S.H.; Wang, Z.Y.; Jiang, H.F. 1, 1-Diphenylvinylsulfide as a Functional AIEgen Derived from the Aggregation-Caused-Quenching Molecule 1, 1-Diphenylethene through Simple Thioetherification. *Angew. Chem. Int. Ed.* **2020**, *59*, 2338–2343. [[CrossRef](#)]
137. Zhang, Z.; Fang, X.; Liu, Z.; Liu, H.; Chen, D.; He, S.; Zheng, J.; Yang, B.; Qin, W.; Zhang, X. Semiconducting Polymer Dots with Dual-Enhanced NIR-IIa Fluorescence for Through-Skull Mouse-Brain Imaging. *Angew. Chem. Int. Ed.* **2020**, *59*, 3691–3698. [[CrossRef](#)]
138. Wu, C.; Chiu, D.T. Highly fluorescent semiconducting polymer dots for biology and medicine. *Angew. Chem. Int. Ed.* **2013**, *52*, 3086–3109. [[CrossRef](#)]
139. Wu, C.; Schneider, T.; Zeigler, M.; Yu, J.; Schiro, P.G.; Burnham, D.R.; McNeill, J.D.; Chiu, D.T. Bioconjugation of ultrabright semiconducting polymer dots for specific cellular targeting. *J. Am. Chem. Soc.* **2010**, *132*, 15410–15417. [[CrossRef](#)]
140. Gao, M.; Tang, B.Z. Fluorescent sensors based on aggregation-induced emission: Recent advances and perspectives. *ACS Sens.* **2017**, *2*, 1382–1399. [[CrossRef](#)]
141. Tsai, W.-K.; Wang, C.-I.; Liao, C.-H.; Yao, C.-N.; Kuo, T.-J.; Liu, M.-H.; Hsu, C.-P.; Lin, S.-Y.; Wu, C.-Y.; Pyle, J.R. Molecular design of near-infrared fluorescent Pdots for tumor targeting: Aggregation-induced emission versus anti-aggregation-caused quenching. *Chem. Sci.* **2019**, *10*, 198–207. [[CrossRef](#)]
142. Luo, J.; Xie, Z.; Lam, J.W.; Cheng, L.; Chen, H.; Qiu, C.; Kwok, H.S.; Zhan, X.; Liu, Y.; Zhu, D. Aggregation-induced emission of 1-methyl-1, 2, 3, 4, 5-pentaphenylsilole. *Chem. Commun.* **2001**, *18*, 1740–1741. [[CrossRef](#)] [[PubMed](#)]
143. Qi, J.; Sun, C.; Zebibula, A.; Zhang, H.; Kwok, R.T.; Zhao, X.; Xi, W.; Lam, J.W.; Qian, J.; Tang, B.Z. Real-time and high-resolution bioimaging with bright aggregation-induced emission dots in short-wave infrared region. *Adv. Mater.* **2018**, *30*, 1706856. [[CrossRef](#)] [[PubMed](#)]
144. Sheng, Z.; Guo, B.; Hu, D.; Xu, S.; Wu, W.; Liew, W.H.; Yao, K.; Jiang, J.; Liu, C.; Zheng, H. Bright aggregation-induced-emission dots for targeted synergetic NIR-II fluorescence and NIR-I photoacoustic imaging of orthotopic brain tumors. *Adv. Mater.* **2018**, *30*, 1800766. [[CrossRef](#)] [[PubMed](#)]
145. Li, Y.; Hu, D.; Sheng, Z.; Min, T.; Zha, M.; Ni, J.-S.; Zheng, H.; Li, K. Self-assembled AIEgen nanoparticles for multiscale NIR-II vascular imaging. *Biomaterials* **2021**, *264*, 120365. [[CrossRef](#)]
146. Fang, Y.; Shang, J.; Liu, D.; Shi, W.; Li, X.; Ma, H. Design, synthesis, and application of a small molecular NIR-II fluorophore with maximal emission beyond 1200 nm. *J. Am. Chem. Soc.* **2020**, *142*, 15271–15275. [[CrossRef](#)] [[PubMed](#)]
147. Ye, F.; Huang, W.; Li, C.; Li, G.; Yang, W.C.; Liu, S.H.; Yin, J.; Sun, Y.; Yang, G.F. Near-Infrared Fluorescence/Photoacoustic Agent with an Intensifying Optical Performance for Imaging-Guided Effective Photothermal Therapy. *Adv. Ther.* **2020**, *3*, 2000170. [[CrossRef](#)]
148. Rao, R.S.; Singh, S.P. Near-Infrared (>1000 nm) Light-Harvesters: Design, Synthesis and Applications. *Chem. Eur. J.* **2020**, *26*, 16582–16593. [[CrossRef](#)]
149. Wang, Y.; Wang, M.; Xia, G.; Yang, Y.; Si, L.; Wang, H.; Wang, H. Maximal Emission beyond 1200 nm Dicyanovinyl-Functionalized Squaraine for in vivo Vascular Imaging. *Chem. Commun.* **2023**, *59*, 3598–3601. [[CrossRef](#)]
150. Tu, L.; Xu, Y.; Ouyang, Q.; Li, X.; Sun, Y. Recent advances on small-molecule fluorophores with emission beyond 1000 nm for better molecular imaging in vivo. *Chin. Chem. Lett.* **2019**, *30*, 1731–1737. [[CrossRef](#)]
151. Zhang, X.D.; Wang, H.; Antaris, A.L.; Li, L.; Diao, S.; Ma, R.; Nguyen, A.; Hong, G.; Ma, Z.; Wang, J. Traumatic brain injury imaging in the second near-infrared window with a molecular fluorophore. *Adv. Mater.* **2016**, *28*, 6872–6879. [[CrossRef](#)]
152. Antaris, A.L.; Chen, H.; Diao, S.; Ma, Z.; Zhang, Z.; Zhu, S.; Wang, J.; Lozano, A.X.; Fan, Q.; Chew, L. A high quantum yield molecule-protein complex fluorophore for near-infrared II imaging. *Nat. Commun.* **2017**, *8*, 15269. [[CrossRef](#)] [[PubMed](#)]
153. Feng, Y.; Zhu, S.; Antaris, A.L.; Chen, H.; Xiao, Y.; Lu, X.; Jiang, L.; Diao, S.; Yu, K.; Wang, Y. Live imaging of follicle stimulating hormone receptors in gonads and bones using near infrared II fluorophore. *Chem. Sci.* **2017**, *8*, 3703–3711. [[CrossRef](#)] [[PubMed](#)]
154. Kalay, S.; Stetsyshyn, Y.; Donchak, V.; Harhay, K.; Lishchynskiy, O.; Ohar, H.; Panchenko, Y.; Voronov, S.; Çulha, M. pH-Controlled fluorescence switching in water-dispersed polymer brushes grafted to modified boron nitride nanotubes for cellular imaging. *Beilstein J. Nanotechnol.* **2019**, *10*, 2428–2439. [[CrossRef](#)] [[PubMed](#)]
155. Nese, A.; Lebedeva, N.V.; Sherwood, G.; Averick, S.; Li, Y.; Gao, H.; Peteanu, L.; Sheiko, S.S.; Matyjaszewski, K. pH-responsive fluorescent molecular bottlebrushes prepared by Atom Transfer Radical polymerization. *Macromolecules* **2011**, *44*, 5905–5910. [[CrossRef](#)]
156. Liu, S.; de Beer, S.; Batenburg, K.M.; Gojzewski, H.; Duvigneau, J.; Vancso, G.J. Designer Core-Shell Nanoparticles as Polymer Foam Cell Nucleating Agents: The Impact of Molecularly Engineered Interfaces. *ACS Appl. Mater. Interfaces* **2021**, *13*, 17034–17045. [[CrossRef](#)] [[PubMed](#)]

157. Chen, Y.; Xu, H.; Ma, Y.; Liu, J.; Zhang, L. Diffusion of polymer-grafted nanoparticles with dynamical fluctuations in unentangled polymer melts. *Phys. Chem. Chem. Phys.* **2022**, *24*, 11322–11335. [[CrossRef](#)]
158. Xia, C.; Zhu, S.; Feng, T.; Yang, M.; Yang, B. Evolution and synthesis of carbon dots: From carbon dots to carbonized polymer dots. *Adv. Sci.* **2019**, *6*, 1901316. [[CrossRef](#)]
159. Ru, Y.; Ai, L.; Jia, T.; Liu, X.; Lu, S.; Tang, Z.; Yang, B. Recent advances in chiral carbonized polymer dots: From synthesis and properties to applications. *Nano Today* **2020**, *34*, 100953. [[CrossRef](#)]
160. Pan, K.; Liu, C.; Zhu, Z.; Feng, T.; Tao, S.; Yang, B. Soft–Hard Segment Combined Carbonized Polymer Dots for Flexible Optical Film with Superhigh Surface Hardness. *ACS Appl. Mater. Interfaces* **2022**, *14*, 14504–14512. [[CrossRef](#)]
161. Liu, J.; Li, R.; Yang, B. Carbon dots: A new type of carbon-based nanomaterial with wide applications. *ACS Cent. Sci.* **2020**, *6*, 2179–2195. [[CrossRef](#)]
162. Zeng, Q.; Feng, T.; Tao, S.; Zhu, S.; Yang, B. Precursor-dependent structural diversity in luminescent carbonized polymer dots (CPDs): The nomenclature. *Light Sci. Appl.* **2021**, *10*, 142. [[CrossRef](#)] [[PubMed](#)]
163. Lou, K.; Hu, Z.; Zhang, H.; Li, Q.; Ji, X. Information Storage Based on Stimuli-Responsive Fluorescent 3D Code Materials. *Adv. Funct. Mater.* **2022**, *32*, 2113274. [[CrossRef](#)]
164. Battistelli, G.; Cantelli, A.; Guidetti, G.; Manzi, J.; Montalti, M. Ultra-bright and stimuli-responsive fluorescent nanoparticles for bioimaging. *Wiley Interdiscip. Rev. Nanomed. Nanobiotech.* **2016**, *8*, 139–150. [[CrossRef](#)] [[PubMed](#)]
165. Mazrad, Z.A.I.; Lee, K.; Chae, A.; In, I.; Lee, H.; Park, S.Y. Progress in internal/external stimuli responsive fluorescent carbon nanoparticles for theranostic and sensing applications. *J. Mater. Chem. B* **2018**, *6*, 1149–1178. [[CrossRef](#)] [[PubMed](#)]

Disclaimer/Publisher’s Note: The statements, opinions and data contained in all publications are solely those of the individual author(s) and contributor(s) and not of MDPI and/or the editor(s). MDPI and/or the editor(s) disclaim responsibility for any injury to people or property resulting from any ideas, methods, instructions or products referred to in the content.